GEOCHEMICAL EVIDENCE FOR LOCAL VARIABILITY IN REDOX AND DEPOSITIONAL CONDITIONS IN A DEEP-WATER BONARELLI EQUIVALENT SECTION FROM SOUTHERN TETHYS (FONTANA VALLONETO SECTION, SOUTHERN ITALY)

Greta Bonacina*,,✉, Alessio Sanfilippo*,***, Simone Zana*, Alberto Bosino*, Elisabetta Previde Massara**, Paolo Viaggi**, Luisa Sabato°, Salvatore Gallicchio°** and **Paolo Scotti****

* *Department of Earth and Environmental Sciences, University of Pavia, Italy.*
** *Eni S.p.A. Upstream Research and Technological Innovation, San Donato Milanese, MI, Italy.*
*** *IGG-Istituto Geoscienze e Georisorse, CNR, U.O. Pavia, Italy.*
° *Department of Earth and Geo-environmental Sciences, University of Bari Aldo Moro, Bari, Italy.*
✉ *Corresponding author, email: greta.bonacina01@universitadipavia.it*

Keywords: *redox conditions; Bonarelli Level; trace metals geochemistry; OAE 2; TOC; Radiolarians; Cretaceous; Fontana Valloneto; Southern Italy.*

ABSTRACT

Identifying the depositional redox conditions is useful to evaluate the interplay between climate changes, biological feedbacks and de-oxygenation processes in the oceans during the Oceanic Anoxic Events (OAEs). Here, we focus on the about 56 m-thick Albian-Turonian Fontana Valloneto stratigraphic section cropping out in Southern Italy (Potenza, Basilicata), belonging to the "Flysch Rosso" Formation, and containing an equivalent of the Bonarelli Horizon (globally called OAE2 which occurred at~ 94 Ma). Inorganic geochemical compositions and Total Organic Carbon contents obtained from this section are here used to assess depositional environment and redox conditions. The paucity of carbonates within the entire sequence and a gradual decrease in Y, Zr and Al contents along the section suggest a deep depositional environment (below the Calcite Compensation Depth) and an overall decrease in the terrigenous supply. Samples within the Bonarelli Horizon (BH-e) show highly variable TOC contents (~ 0 to ~ 30 wt%) that, mirrored by variations in redox sensitive and nutrient-related elements (e.g. V, Mo and U) and Mn, suggest variation of the seawater primary productivity associated to changes of the local redox conditions between suboxic to strongly euxinic. We infer that during OAE2 the accumulation of the black shales was associated to high Organic Matter (OM) productivity, high biogenic silica production and fine-grained sedimentation (mainly aeolian dust and illite) in a period of "sluggish" oceanic circulation and stagnant conditions. These periods were alternated by moments of more active oceanic circulation and enhanced runoff, leading to the local deposition of radiolarites with very low TOC contents. Finally, a comparison with other section from the proto-Atlantic Ocean and the Mesozoic Tethys sustains the idea that the drawdown of redox-sensitive elements (V, Mo and U) was a global process during the deposition of OAE2, providing a link between the environmental changes detected in our section with the global perturbations developed during this oceanic anoxic event.

INTRODUCTION

Cretaceous deep marine sediments are widely exposed along the outer margin of the Southern Apennines, in Lucania and Sannio regions. These deposits, well-known as "argille varicolori" (Auctt.) are made up mainly of clayshales with rare limestone intercalations, and dark organic matter-rich interbedded layers, corresponding to "black shales" (Gallicchio et al., 1996). Since the preservation of organic matter is substantially dependent on anoxic conditions, many authors related these black-shale layers to oxygen-depleted conditions (Schlanger and Jenkyns, 1976). Likewise, the discovery of coeval black shale layers in several IODP sites in modern oceanic basins led to the idea that the deposition of these sediments was related to global anoxic conditions (Takashima et al., 2006). Such events were thus called "Oceanic Anoxic Events" (OAEs) after Schlanger and Jenkyns (1976).

One of the most studied anoxic events is arguably the Oceanic Anoxic Event 2 (OAE 2; Beaudoin et al., 1996; Turgeon and Brumsack, 2006; Lanci et al., 2010; Gambacorta et al., 2015), which occurred at the Cenomanian-Turonian boundary (~ 93.9 Ma after Cohen et al., 2013), lasting between 450 and 900 kyrs (see also Arthur and Premoli-Silva, 1982; Kuhnt et al., 2005; Sageman et al., 2006; Voigt et al., 2008; Eldrett et al., 2015; Batenburg et al., 2016). The sedimentary record of this event is generally called 'Bonarelli Level' in its typical outcrop section along the Bottaccione Section (Gubbio, Central Italy) (Jenkyns, 1985; Schlanger et al., 1987; Arthur et al., 1990; Jenkyns, 2003; Scopelliti et al., 2004; 2006; Kuroda et al., 2007). The Bonarelli Level is lithologically identified by intensely stratified black shales with severe enrichments in TOC (> 15 wt%) (e.g. Sabato et al., 2007). Several authors postulated that this period also coincided with severe global climatic perturbations and greenhouse conditions (Schlanger et al., 1987; Takashima et al., 2006; Jenkyns, 2010), characterized high CO_2 levels in atmosphere (Berner, 2006; Takashima et al., 2006; Friedrich et al., 2012). These conditions were likely caused by elevated volcanic activity (Kuroda et al., 2007; Jenkyns, 2010) followed by high sea levels (Haq et al., 1987; Jarvis et al., 2001), high seawater temperature (Jenkyns, 2010, Owens et al., 2017), lack of permanent ice sheets (Takashima et al., 2006), strong increase in the production, accumulation and preservation of marine and terrestrial organic matter (Scholle and Arthur, 1980; Arthur et al., 1990; Hasegawa, 1997). The perturbation in the carbon cycle are proved by strong excursions in the stable carbon isotopes ($\delta^{13}C$), in turn triggered by intense weathering (Blättler et al., 2011; Blumenberg and Wiese, 2012; Pogge Von Strandmann et al., 2013), increased hydrothermal activity (Jones and Jenkyns, 2001; Du Vivier et al.,

2014, 2015) and changes in oceanic circulation (Takashima et al., 2006; Martin et al., 2012).

On a paleoceanographic perspective, the OAE2 was characterized by widespread anoxia and local euxinic conditions as it has been observed in many locations (Turgeon and Brumsack, 2006; Jenkyns et al., 2007; Pearce et al., 2009; Lu et al., 2010; Hetzel et al., 2011; Owens et al., 2012, 2016; Westermann et al., 2014; Dickson et al., 2016a: 2016b; Goldberg et al., 2016; Ostrander et al., 2017). During this event, euxinia caused the drawdown of bio-essential metals, such as Mo and V, which are preferentially retained in the organic matter-rich sediments (Algeo and Maynard, 2004; Reinhard et al., 2013; Goldberg et al., 2016; Owens et al., 2016; Ostrander et al., 2017).

In this work, we characterize a sedimentary section of Cenomanian-Turonian age cropping out near the town of Vaglio di Basilicata in Southern Italy (Fig. 1). This section intersects a Bonarelli Horizon-equivalent (BH-e) ~ 2 meters-thick. Organic features (Total Organic Carbon, TOC and Hydrogen Index, HI), biostratigraphy and facies of this horizon have been already studied in detail by Sabato et al. (2007). Now, we combine their data with a new dataset including mineralogy, major and trace element compositions, with the goal of constraining redox and depositional conditions in the depositional environment before, during and after the BH-e sedimentation. Specifically, this multi-proxy approach allows us to constrain the paleo environmental changes occurred at the Cenomanian-Turonian boundary in a poorly-known Bonarelli equivalent section of Southern Tethys located in deep waters. In addition, the comparison with other sections of the Tethys and of the proto-Atlantic Ocean allowed a better understanding of the paleo-oceanographic conditions during the

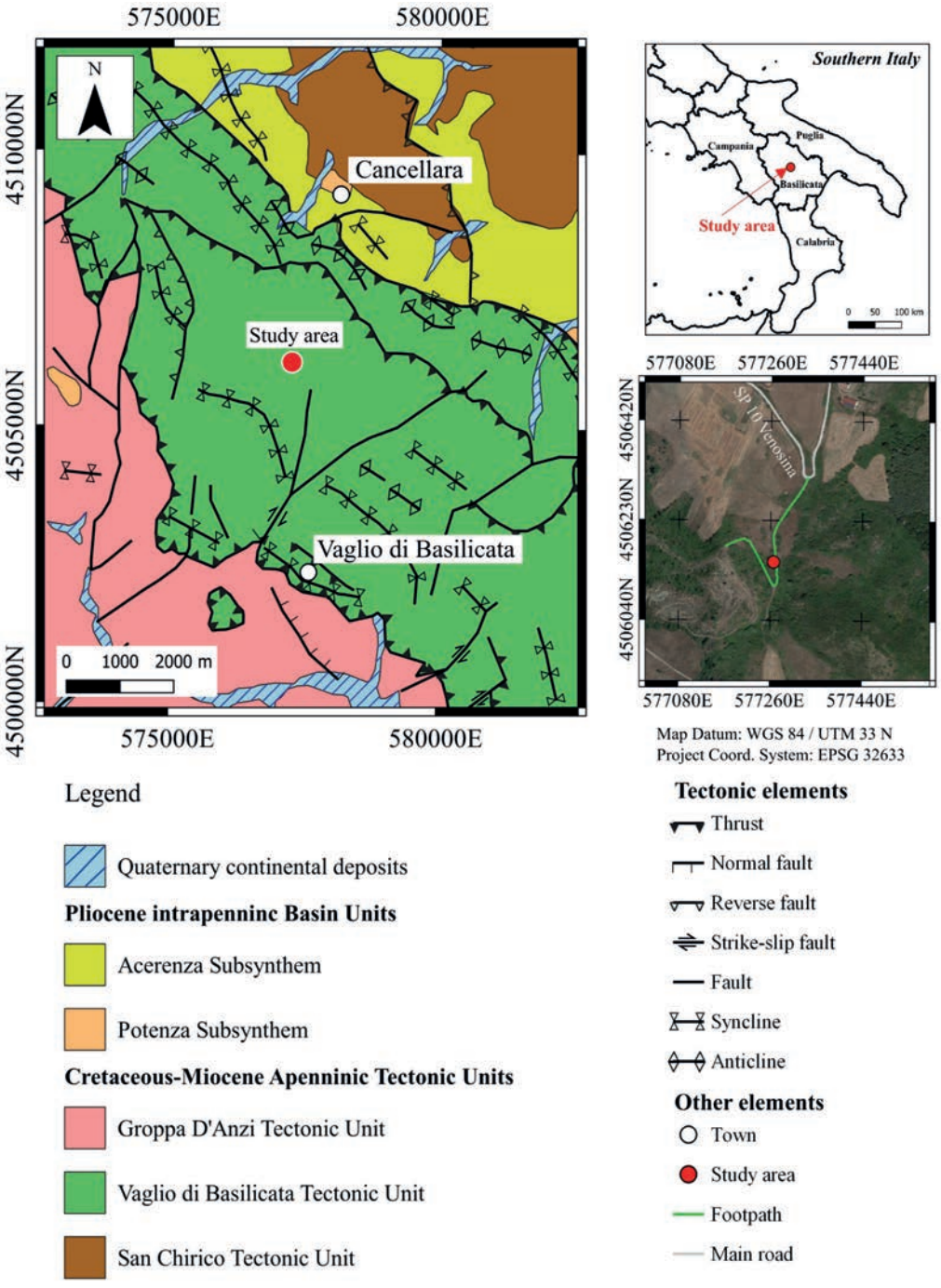

Fig. 1 - Tectonic setting of the study area (modified from ISPRA, in press) and outcrop location.

OAE2, confirming the global environmental perturbations (e.g. nutrient crisis, expanded anoxia in bottom waters, stagnant conditions, drawdown of bio-essential trace elements) occurred during this period.

STUDY AREA

The study area (Fig. 1) is located between Vaglio di Basilicata and Cancellara villages, NE of Potenza, on the easternmost thrust edge of the Southern Apennines. In the study area, from top to bottom, three different tectonic units have been identified (ISPRA, 2017; in press; Pieri et al., 2017; Pescatore et al., in press): Groppa d'Anzi, Vaglio di Basilicata and San Chirico tectonic units (Fig. 1).

The Groppa d'Anzi Tectonic Unit represents the inner margin of the middle Miocene Southern Apennines foredeep system, i.e. the allochthonous units of the early-middle Miocene thrust edge of the Southern Apennines and the overlying wedge-top deposits (Pescatore et al., 1999). The Vaglio di Basilicata Tectonic Unit is constituted by the Cretaceous-Miocene succession of the Lagonegro–Molise Basin *sensu* Mostardini and Merlini (1986). From the bottom to the top this unit includes Flysch Galestrino, Flysch Rosso and Flysch Numidico formations; the Flysch Galestrino is poorly represented while the Flysch Rosso outcrops widely. The San Chirico Tectonic Unit is made up of three formations: Flysch Rosso, Flysch Numidico and Serra Palazzo Formation. Its Cretaceous – middle Miocene sedimentary succession is mainly represented by Serra Palazzo Formation belonging to the middle Miocene Southern Apennines Foredeep (e.g. Pescatore and Senatore, 1986; Gallicchio and Maiorano, 1999).

The studied succession crops out close to Vaglio di Basilicata (Fig. 1) and constitutes the detachment layer of the Vaglio di Basilicata Tectonic Unit. Locally, the Flysch Galestrino is not represented and this tectonic unit can be subdivided, from the bottom, into three stratigraphic units:

The lower unit, represented by varicoloured shale deposits interbedded with radiolarian-rich mudstones and black shale ("argilliti e radiolariti di Campomaggiore" *sensu* Sabato et al., 2007, lower part of Flysch Rosso, *auctt*.), includes the "argilliti varicolori" and the "diaspri" (*sensu* Centamore et al., 1971a and 1971b), and contains the Bonarelli Horizon-equivalent (Gallicchio et al., 1996; Sabato et al., 2007) which is related to the late Cretaceous Oceanic Anoxic Events OAE 2 (Schlanger and Jenkyns, 1976; Arthur et al., 1990).

The intermediate unit consists of hemipelagic and clastic resedimented limestones with interbedded Cretaceous-early Miocene red marls and clays; this unit comprises the "calcareniti e argilliti rosse di Fontana Valloneto" *sensu* Centamore et al. (1971a; b) and corresponds to the middle and upper part of Flysch Rosso (Sabato et al., 2007).

The upper unit corresponds to the Burdigalian-early Langhian Flysch Numidico (e.g. Ogniben, 1969; Ciaranfi and Loiacono, 1983; Patacca et al., 1992; Gallicchio et al., 1996; Guerrera et al., 2012). This formation is represented by yellowish quartz-rich arenites with interbedded brownish grey clays, exclusively fed by the African Craton (e.g. Fornelli et al., 2019; Butler et al., 2020), and represents the first siliciclastic input in the Lagonegro-Molise Basin.

The lower unit, well exposed in the Fontana Valloneto section, was firstly attributed to the Cretaceous–Eocene Sicilidi Units ("Argille Variegate" *sensu* Ogniben, 1969) and then to more external units belonging to the Lagonegro–Molise Basin (late Cretaceous– early Miocene; "argilliti varicolori" *sensu* Mostardini and Merlini, 1986; "Fysch Rosso esterno" *sensu* Pescatore et al., 1988; "argilliti e radiolariti di Campomaggiore", *sensu* Sabato et al., 2007). Successively, the "argilliti e radiolariti di Campomaggiore" and the intermediate unit of the Vaglio di Basilicata Tectonic Unit were formally grouped into a single formation (Flysch Rosso), in turn subdivided, from bottom, in two members: "membro diasprigno" and "membro calcareo" (APAT, 2006).

The Fontana Valloneto stratigraphic section is located along a slope on the north-eastern limb of a syncline with a NW-SE striking axial plane (Figs. 1 and 2). Generally, the section consists of reddish shale, laminated and fissile, interbedded with greenish shale (Fig. 2) indicating that the depositional environment was located in a deep-sea basin for the entire interval represented by the section. The biostratigraphic micropaleontological assemblage has allowed to Sabato et al. (2007) to attribute an age spanning from lower Albian to Turonian to the Fontana Valloneto sedimentary succession (~100 – 90 Ma).

Specifically, this section, as described by Sabato et al. (2007), can be divided into two portions separated by an about 15 m-thick zone covered by vegetation. The lower 37 m-thick part, early-middle Albian in age, is mainly made up of reddish siliceous claystone/clayshales with minor green and grey interbedded layers. Their beds are some centimeters up to a few decimeters thick and show dense parallel- and ripple laminations. Some very thin layers (a few centimeters) of black shales stand out due to the presence of Fe–Mn oxyhydroxides; one of these layers, characterized by a TOC content of ~ 3.5 wt%, was referred by the authors to an organic enriched event called "Valloneto Albian Event 1" (VAE1, sample V13A, in Fig. 2). Sabato et al. (2007) showed that in this part of the section (samples V0A-V16B in Fig. 2), radiolarians (such as: *Dictyomitra montisserei, Dictyomitra gracilis, Dictyomitra pulchra* and *Thanarla brouweri*) are present in the green claystones/clayshales, where they are well preserved. Conversely, in the red shales and black shales, radiolarians and other microfossils are absent.

The upper part of the section, of Cenomanian-Turonian in age, is about 6 m-thick, and is divisible in three portions. The lowermost portion (~1,3 m thick; samples V16D-V20A in Fig. 2) is mainly represented by thinly bedded red radiolarian-rich mudstone and claystones/clayshales. The age of this part of the section has been attributed to the Cenomanian thanks to the radiolarian assemblages constituted mainly by *Dactyliosphaera silviae, Pseudodictyomitra tiara, Thanarla pulchra, Thanarla veneta, Novixitus mclaughlini, Rhopalosyringium majourensis, Rhopalosyringium petilum* and *Guttacapsa gutta* (lower radiolarian assemblage samples V17 – V25, Sabato et al., 2007). The intermediate portion is about 2.3 m-thick (samples V21-V37A in Fig. 2, Fig. 3) and is mainly composed of centimeter-thick layers of grey and green dark siliceous mudstones (Fig. 3C) with interbedded green siliceous clayshales and black shales (Fig. 3B) and very rare limestones (Fig. 2). This portion shows a very high amount of organic matter with a TOC value spanning from 30 wt% to 41,9 wt%. All the analyzed features allowed the authors to identify the Bonarelli Horizon-equivalent (BH-e) for this part of the section (Figs. 2 and 3), worldwide corresponding to the Oceanic Anoxic Event 2 (OAE 2 *sensu* Schlanger and Jenkins, 1976). Several micropaleontological assemblage changes moving into the BH-e: the Cenomanian species disappear above the samples V25, while the samples V33 – V37 yield typical Turonian radiolarian species (Sabato et al., 2007).

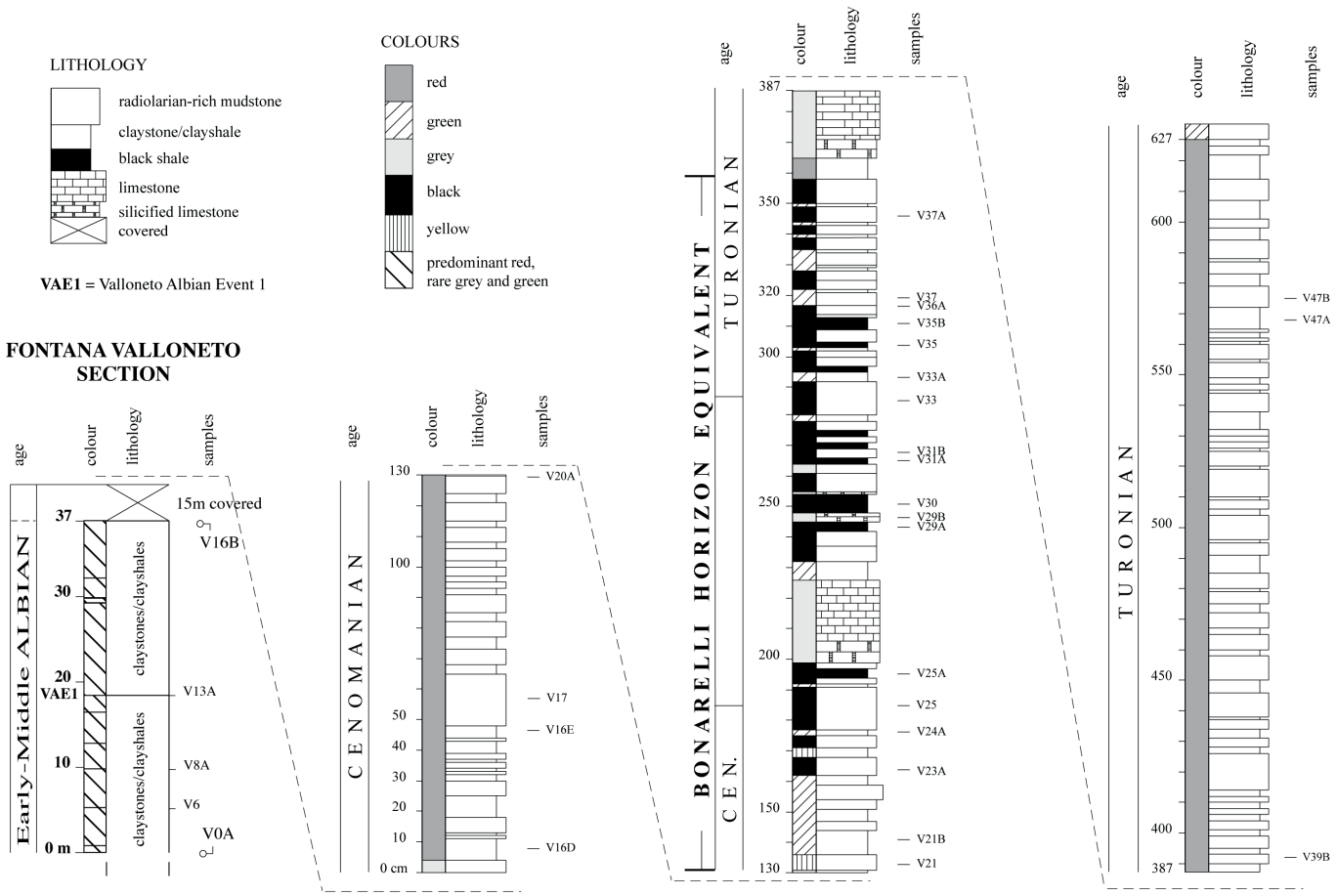

Fig. 2 - Stratigraphy of the Bonarelli Horizon-equivalent along the Fontana Valloneto section (modified from Sabato et al., 2007). Take into consideration the different used scales in the two parts of the section. The samples V17, V25, V33 and V37 have not been analyzed for the inorganic geochemistry in this paper.

Finally, the upper portion, about 2.7 m-thick and Turonian in age (samples V39B-V47B in Fig. 2), represents a continuous sedimentary record, constituted by an alternance of red claystones/clayshales and radiolarian rich-mudstones. Sabato et al. (2007) showed a Turonian radiolarian assemblages into this portion, constituted by *Crucella cachensis, Hemicryptocapsa polyhedra, Acanthocircus hueyi* and *Alievium superbum*.

MATERIAL AND METHODS

Sampling

Thirty-nine surface samples have been selected for the mineralogical and chemical characterization from the collection of Sabato et al., (2007) (Fig. 2) spanning the entire section. 17 samples (from V0A to V16B) have been collected in the lower part of the section, Early-Middle Albian in age. Three samples (from V16D to V20A) have been collected in the middle part of the interval. These samples are of Cenomanian age and are older than the BH-e. Owning to the BH-e along the Cenomanian-Turonian boundary, 16 samples (from V21 to V37A) have been selected. Finally, in the upper part of the succession three samples (from V39B to V47B) of Turonian age have been selected. Lithology and colour of each sample are represented in Fig. 2. We must note, however, that the poor field exposure prevented to collect representative samples from late Albian to early Cenomanian (~ 15m; see Fig. 2).

Analytical methodologies and techniques

Organic geochemical data (TOC and HI) are from Sabato et al. (2007). Mineralogical and chemical analyses were performed at the Geolab of Eni S.p.a. in San Donato Milanese (Italy). Selected samples were disaggregated and finely grinded with W-Cr mortar. Fused beams using a $Li_2B_4O_7$ flux and pressed pellets were obtained from each pulverized sample. Major and trace element compositions were obtained by X-ray fluorescence (XRF) on fused beams and pressed pellets, respectively. Mineralogy was acquired by X-ray diffraction (XRD) on X-ray Powder Diffraction (XRPD).

Mineralogical composition was determined by X-ray Powder Diffraction (XRPD) using a Panalytical Cubi'X instrument equipped with a CuKα (λ = 1.54178 Å) radiation source and a Fast detector. The data have been collected in the spectral interval $3° \leq 2\theta \leq 70°$ with steps of 0.02° 2θ and accumulation times of 10s/step. The quantitative bulk analysis was carried out by means of a full-profile fitting procedure based on the Rietveld method. The high accuracy of the spectra at low 2θ angle (the spectra starts from 2° 2θ) has allowed to distinguish between the clayey phases (especially between kaolinite and chlorite) without any pre-treatments of the samples.

Major and trace element concentrations were determined using a Wavelength Dispersive X-Ray Fluorescence System (Panalytical Magix Pro). The chemical data have been used to check the quality of the mineralogical data by XRD.

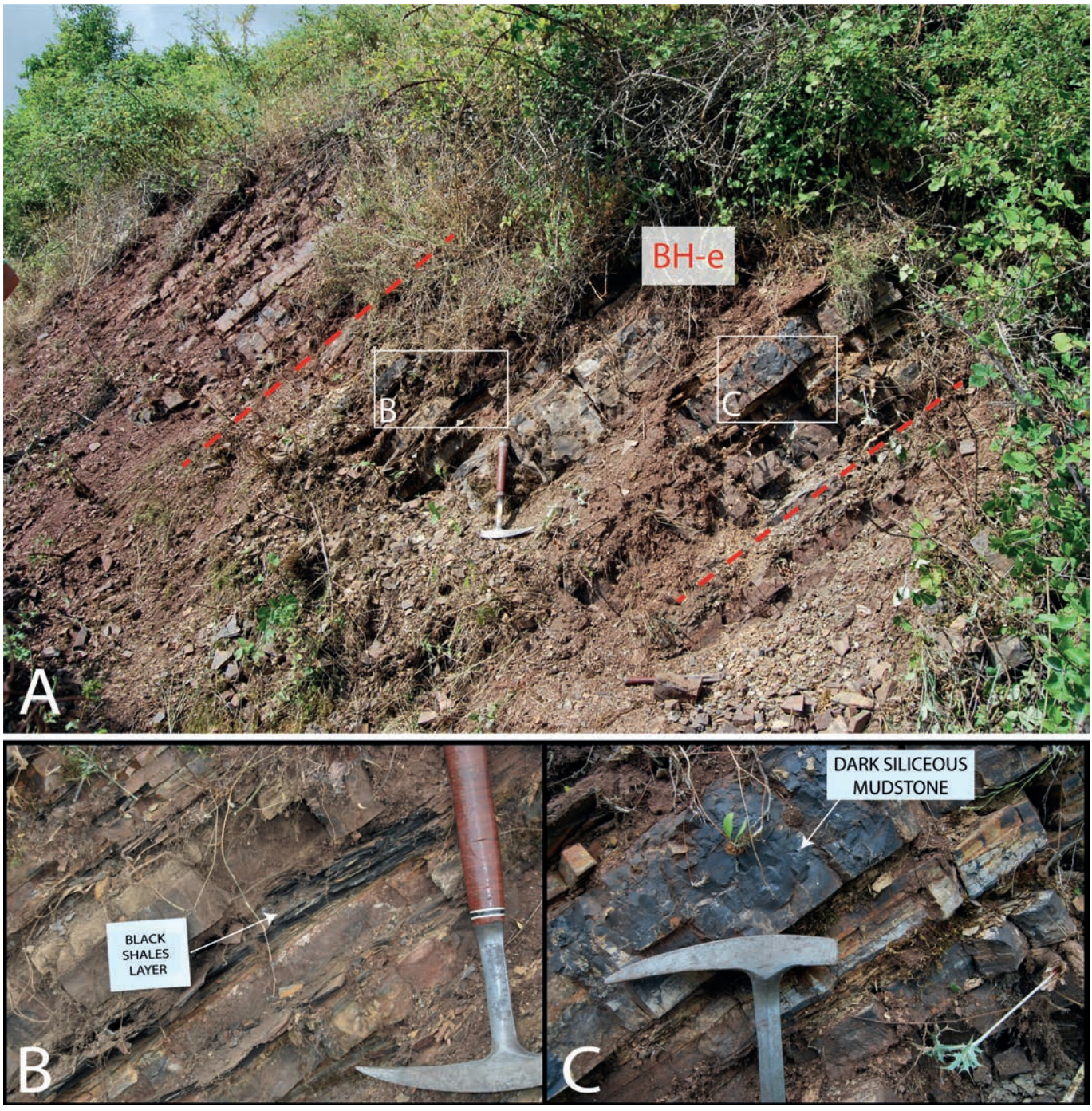

Fig. 3 - A) Outcrop of the upper part of the Fontana Valloneto section containing the Bonarelli Horizon – equivalent (Fig. 3); B) layer of black shales in the Bonarelli Horizon - equivalent; C) dark siliceous mudstone in the Bonarelli Horizon - equivalent.

RESULTS

Mineralogy

Table 1 shows the mineralogical composition of selected samples, and also include the TOC values from Sabato et al. (2007) normalized to 100 wt%. The section is composed mainly by quartz, micas and clays (illite type, kaolinite, vermiculite and chlorite) and other minor phases (goethite, gypsum, fluorapatite, pyrite, plagioclase). Importantly, quartz increases from the bottom to the top of the section with an initial average of ~ 55 wt% prior to, ~ 63 wt% during and ~ 75 wt% after the BH-e. On the contrary, micas and clays decrease along the section from an average of ~ 37 wt% before the BH-e to ~ 18 wt% after the anoxic event. In particular, illite type increases upward from an average of ~ 3 wt% before the BH-e to ~ 6 wt% during the anoxic event, while after the event it decreases until zero. Kaolinite shows an average of ~ 10 wt% prior to the BH-e, ~ 1 wt% during and ~ 2 wt% after the anoxic event. Also, muscovite shows a similar behaviour to kaolinite, varying between ~ 12 and 10 wt% along the section. Chlorite contents are mostly close to zero; however some sample randomly scattered in the section show contents up to ~ 21 wt%. In BH-e, a little amount of fluorapatite is present (up to ~ 7.5 wt%). Significant amounts

Table 1 - Mineralogical content of the section normalized to TOC (wt%). Pyrite contents are underestimated (see discussion in chapter 5.1). The grey area represents the BH-e interval. Mineral names are represented in the abbreviated form (Whitney and Evans, 2010): (Cal) calcite, (Qz) quartz, (Pl) plagioclase, (Ilt type) illite type, (Kln) kaolinite, (Ms) muscovite, (Vrm) vermiculite, (Chl) chlorite, (Py) pyrite, (Hem) hematite, (Gth) geothite, (Gp) gypsum, (Hl) halite and (FAp) fluorapatite.

Sample name	(m)	TOC (wt%)	Cal (wt%)	Qz (wt%)	Pl (wt%)	Ilt type (wt%)	Kln (w%)	Ms (wt%)	Vrm (wt%)	Chl (wt%)	Py (wt%)	Hem (wt%)	Gth (wt%)	Gp (wt%)	Hl (wt%)	FAp (wt%)
V47B	57.8	0.03	-	89.1	-	-	1.7	4.5	0.7	-	-	4.2	-	-	-	-
V47A	57.7	0.02	-	55.1	5.5	6.4	4.8	12.7	5.4	3.7	1.3	5.2	-	-	-	-
V39B	55.9	0.02	-	83.6	-	-	-	14.8	0.4	-	-	1.0	-	-	-	-
V37A	55.5	0.02	-	93.6	-	6.4	-	-	-	-	-	-	-	-	-	-
V36A	55.2	2.44	-	88.4	-	9.2	-	-	-	-	-	-	-	-	-	-
V35B	55.1	25.81	-	35.3	4.2	15.1	-	10.7	7.9	0.1	-	-	0.9	-	-	-
V35	55.1	29.19	-	33.2	2.0	-	-	5.8	23.9	0.7	3.1	-	-	2.3	-	-
V33A	54.9	0.05	-	66.2	5.4	7.1	2.0	16.0	1.5	1.9	-	-	-	-	-	-
V31B	54.7	0.73	-	85.1	-	10.9	-	-	3.2	-	0.3	-	-	-	-	-
V31A	54.7	23.77	-	22.4	0.8	2.4	-	6.6	10.1	14.8	-	-	19.2	-	-	-
V30	54.5	25.50	-	43.2	4.9	4.6	5.0	6.8	1.3	4.6	0.2	0.4	-	2.8	0.1	0.8
V29B	54.5	1.60	-	90.7	-	6.6	-	-	-	-	0.9	-	-	-	-	-
V29A	54.4	16.03	-	61.0	3.9	6.0	0.4	-	10.5	2.1	-	-	-	-	-	-
V25A	54.0	26.52	-	41.3	3.3	10.5	6.9	7.4	0.4	1.5	1.0	0.9	-	-	-	0.7
V24A	53.8	0.05	-	41.9	6.0	12.9	2.8	8.4	17.3	2.0	-	1.3	-	-	-	7.5
V23A (dark)	53.7	3.22	-	78.4	-	-	-	15.2	-	-	-	0.1	-	-	-	3.1
V23A (light)	53.6	0.01	-	95.7	-	-	-	4.1	0.2	-	-	-	-	-	-	-
V21B	53.4	0.08	-	47.5	5.8	7.3	-	12.9	21.1	4.1	-	1.3	-	-	-	-
V21	53.4	0.01	-	84.8	-	-	-	-	4.5	-	-	-	10.7	-	-	-
V20A	53.3	0.02	6.9	73.8	3.9	2.4	3.4	7.9	1.2	-	-	-	-	0.3	-	-
V16E	52.5	0.01	3.1	54.4	1.7	-	-	20.7	10.5	0.6	-	6.9	-	1.9	-	-
V16D	52.1	0.01	-	46.7	4.5	2.8	9.7	25.3	5.1	0.2	-	5.5	-	-	-	-
V16B	37.0	0.02	-	56.8	6.0	10.1	0.4	12.0	13.7	1.1	-	-	-	-	-	-
V16A	32.0	0.04	-	42.7	1.2	3.3	28.1	5.3	-	19.5	-	-	-	-	-	-
V15F	31.0	0.02	-	62.8	3.3	2.3	9.3	4.0	18.1	-	-	-	-	-	-	-
V15D	28.0	0.03	-	45.8	5.4	4.3	8.8	16.1	13.1	-	-	6.5	-	-	-	-
V15C	24.0	0.14	-	65.2	3.7	-	8.6	19.8	2.6	-	-	-	-	-	-	-
V15B	22.0	0.02	-	53.1	1.5	-	6.1	14.8	7.3	-	-	-	17.2	-	-	-
V13A	18.0	3.43	-	71.8	3.3	-	7.4	11.0	3.1	-	-	-	-	-	-	-
V12B	15.0	0.05	-	56.1	4.0	4.3	17.0	7.7	11.0	-	-	-	-	-	-	-
V10B	13.0	0.04	-	46.3	0.8	1.1	10.8	8.8	25.8	-	-	6.2	-	-	-	-
V10A	12.0	0.06	-	44.9	4.1	2.3	5.6	14.8	28.4	-	-	-	-	-	-	-
V10	11.0	0.20	-	51.5	3.6	-	9.3	14.6	20.9	-	-	-	-	-	-	-
V8A	10.0	0.04	-	48.5	4.9	5.5	29.6	9.8	0.7	1.0	-	-	-	-	-	-
V6	5.0	0.03	-	47.0	6.2	18.5	6.4	0.3	-	21.1	-	0.6	-	-	-	-
V4A	3.0	0.03	-	66.5	1.1	1.5	14.5	6.3	8.4	1.5	-	-	-	-	-	-
V1	2.0	0.02	-	43.0	-	6.9	16.5	17.0	-	15.7	-	0.9	-	-	-	-
V0B	1.0	0.03	-	53.9	3.1	-	5.0	11.2	16.1	-	-	10.7	-	-	-	-
V0A	0.0	0.06	-	73.5	4.7	-	3.7	15.1	2.8	-	-	-	-	-	-	-

of phases related to surface alteration (vermiculite, gypsum, goethite, hematite) are present. In particular, vermiculite varies from ~ 9 wt% prior to the BH-e and decreases upward (it reaches ~ 2 wt% after the BH-e).

Organic geochemistry

The organic characteristics of the Fontana Valloneto section have been already discussed by Sabato et al. (2007), where an in-depth discussion of the data can be found. Here, we used the TOC values collected by Sabato et al. (2007). The black shales in the BH-e have a very high TOC content (> 10 wt%) and the values from Rock-Eval pyrolysis suggest that these rocks are "immature", therefore they have Petroleum Potential, TOC and HI comparable to the original values. Some samples from other lithofacies of the Bonarelli Horizon (i.e., dark siliceous claystone and black siliceous mudstone samples V23A, V29B, V31B and V36A) have high organic matter contents (TOC between 1 and 10 wt%). The Bonarelli Horizon-equivalent is characterized by a large amount of organic matter for the black shales (the maximum is ~ 29 wt%). Finally, optical analyses on kerogen highlight very high amount (> 80%) of AOM (Amorphous Organic Matter), and values of HI for samples with TOC > 10 wt% are always above 500 mg HC/g TOC (Sabato et al., 2007), indicating the main presence of algal marine organic matter in these layers.

Elements sensitive to redox conditions (RSEs) and Mn

The RSEs (e.g. V, Mo, U) and Mn (concentrations in Table 2) are used as indicators for redox conditions (see discussion). In particular, in Fig. 4, RSEs and Mn are represented using the enrichment factor (EF), in order to smooth the dilution effect by biogenic silica. The EF is defined as $X_{EF} = [(X/Al)_{sample}/(X/Al)_{UCC}]$ (Algeo and Li, 2020), where X and Al stand for the weight concentrations of element X and Al, respectively. Samples were normalized using the Upper Continental Crust (UCC) compositions of McLennan (2001). If X_{EF} is greater than 1, then element X is enriched relative to average shales and, if X_{EF} is less than 1, it is depleted (Tribovillard et al., 2006).

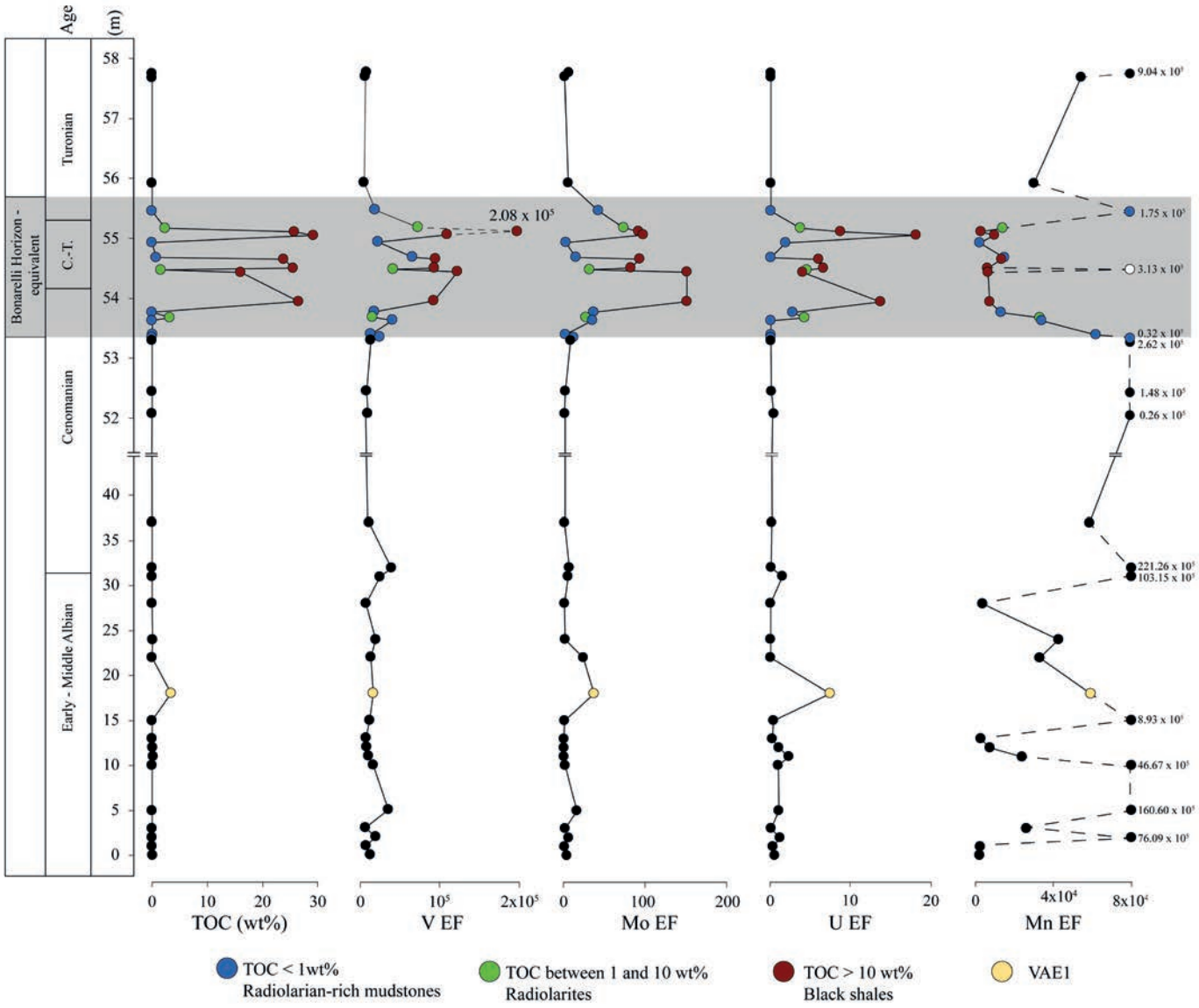

Fig. 4 - Total Organic Carbon (TOC) (values from Sabato et al., 2007) and the enrichment factors of the redox – sensitive elements (V, Mo, U) and Mn. VAE1 stands for "Valloneto Albian Event 1". The white point in the Mn_{EF} graph represents an altered sample with anomalous value of Mn.

Table 2 - RSEs (V, Mo, U), Mn, Y, Zr, Al, Si and Mo/TOC content of the section. The grey area represents the BH-e interval.

Sample name	(m)	V (ppm)	Mn (ppm)	Rb (ppm)	Y (ppm)	Zr (ppm)	Mo (ppm)	U (ppm)	K (wt%)	Ti (wt%)	Al (wt%)	Si (wt%)	TOC (wt%)	Mo/TOC (ppm/wt%)
V47B	57.8	22	14462	17	12	27	3	-	0.45	0.09	2.14	1.00	0.03	N. C.
V47A	57.7	53	2686	83	48	99	3	-	1.82	0.42	6.39	2.99	0.02	N. C.
V39B	55.9	13	482	22	5	23	2	-	0.48	0.07	2.06	0.96	0.02	N. C.
V37A	55.5	16	804	5	2	11	5	-	0.13	0.02	0.62	0.29	0.02	N. C.
V36A	55.2	96	106	10	5	18	14	1	0.24	0.04	0.96	0.45	2.44	5.6
V35B	55.1	1818	148	60	30	76	116	20	2.97	0.55	6.56	3.07	25.81	4.5
V35	55.1	691	346	38	59	58	86	28	1.74	0.36	4.56	2.13	29.19	2.9
V33A	54.9	195	125	102	18	110	5	4	2.18	0.43	6.47	3.02	0.05	N. C.
V31B	54.7	162	207	18	3	35	5	-	0.45	0.09	1.78	0.83	0.73	N. C.
V31A	54.7	726	580	39	23	56	99	11	1.60	0.70	5.51	2.58	23.77	4.2
V30	54.5	624	240	43	18	51	77	11	1.75	0.35	4.83	2.26	25.50	3.0
V29B	54.5	131	5349	19	20	39	14	4	0.52	0.11	2.29	1.07	1.60	8.8
V29A	54.4	584	173	28	12	34	100	5	0.98	0.30	3.45	1.61	16.03	6.2
V25A	54.0	709	327	48	20	66	160	26	2.21	0.49	5.52	2.58	26.52	6.0
V24A	53.8	175	755	108	97	143	53	7	2.55	0.56	7.43	3.47	0.05	N. C.
V23A (dark)	53.7	37	444	18	54	34	9	3	0.43	0.08	1.73	0.81	3.22	2.9
V23A (light)	53.6	53	251	10	9	22	7	-	0.25	0.05	0.95	0.44	0.01	N. C.
V21B	53.4	132	3599	99	35	108	4	-	2.39	0.51	7.53	3.52	0.08	N. C.
V21	53.4	57	4130	10	7	48	4	-	0.38	0.07	1.71	0.80	0.01	N. C.
V20A	53.3	54	59626	27	18	38	6	-	0.84	0.21	3.04	1.42	0.02	N. C.
V16E	52.5	56	59064	68	48	83	3	-	1.57	0.33	5.33	2.49	0.01	N. C.
V16D	52.1	81	13272	86	41	93	3	1	2.04	0.41	6.68	3.12	0.01	N. C.
V16B	37.0	101	3044	64	28	117	3	-	1.60	0.52	6.98	3.26	0.02	N. C.
V16A	32.0	177	541211	33	34	50	5	-	0.76	0.19	3.28	1.53	0.04	N. C.
V15F	31.0	108	242284	29	33	53	4	2	0.69	0.18	3.15	1.47	0.02	N. C.
V15D	28.0	75	226	87	30	123	3	-	1.93	0.53	7.99	3.74	0.03	N. C.
V15C	24.0	145	1756	57	18	105	3	-	1.37	0.41	5.53	2.59	0.14	N. C.
V15B	22.0	80	1069	51	21	89	21	-	1.04	0.27	4.33	2.02	0.02	N. C.
V13A	18.0	93	1836	35	15	87	31	11	0.89	0.32	4.16	1.94	3.43	9.0
V12B	15.0	107	45363	64	20	101	3	1	1.35	0.46	6.80	3.18	0.05	N. C.
V10B	13.0	83	187	82	36	145	3	1	1.72	0.63	8.73	4.08	0.04	N. C.
V10A	12.0	93	490	81	24	128	3	3	1.82	0.58	8.88	4.15	0.06	N. C.
V10	11.0	119	1520	75	21	136	3	7	1.73	0.57	8.47	3.96	0.20	N. C.
V8A	10.0	144	222945	67	47	91	4	2	1.39	0.36	6.40	2.99	0.04	N. C.
V6	5.0	198	486900	44	64	52	14	1	0.68	0.21	4.06	1.90	0.03	N. C.
V4A	3.0	53	1131	52	18	90	3	-	1.03	0.35	5.82	2.72	0.03	N. C.
V1	2.0	155	326109	55	54	85	8	2	1.11	0.33	5.74	2.68	0.02	N. C.
V0B	1.0	79	157	85	30	126	3	1	1.85	0.58	8.58	4.01	0.03	N. C.
V0A	0.0	119	107	74	24	121	7	1	1.68	0.49	7.09	3.31	0.06	N. C.

In our section, values of V, Mo and U are mirrored by increase in TOC (Fig. 4). In detail, during the BH-e deposition, these three elements in sediments were higher than the reference values of the upper continental crust (UCC; McLennan, 2001). The general increase in V, Mo and U with TOC is also observed in the Albian sample V13A (VAE1 in Fig. 4). Mn shows an opposite trend (Fig. 4), decreasing at increasing TOC, which is likely due to the Mn oxides dissolution under reducing conditions (Tribovillard et al., 2006).

Vanadium

In the Fontana Valloneto section, before the BH-e, V is enriched compared to the UCC (V_{UCC} = 107 ppm; McLennan, 2001) as shown by the EF with an average of ~ $1.5x10^4$. During the anoxic event, V_{EF} shows very strong enrichments, with an average value of ~ $6.7x10^4$ and a maximum value of ~ $2.0x10^5$. In the upper part of the section, after the BH-e, V_{EF} shows an average of ~ $6.2x10^3$ (Fig. 4).

Molybdenum

In the Fontana Valloneto section, before the BH-e, molybdenum enrichment factor shows average values of ~ 7.5 ppm, very close to 1. In the BH-e, Mo shows enrichments, indeed, the Mo_{EF} reaches values of ~ 155 ppm (Fig. 4). After the anoxic event, Mo_{EF} shows an average of ~ 5.3.

Uranium

In the lower part of the Fontana Valloneto section, U results depleted compared to the UCC (U_{UCC} = 2.8 ppm; McLennan, 2001) as U_{EF} shows an average lower than 1. During the anoxic event, U_{EF} increases reaching a maximum of ~ 17.7 as shown in Fig. 4. In the samples after the BH-e, U is absent.

Manganese

Mn_{EF} in sediments deposited before the Bonarelli Horizon-equivalent (Late Albian-Cenomanian) is variable between a minimum of ~ $2.0x10^3$ and a maximum of

~ $221.2x10^5$ (Fig. 4). In the latter case, Mn forms microcrystalline or amorphous phases (e.g. oxy - hydroxides) not detected by XRD but visible in the samples by hand (Fig. 5). These phases (e.g. Rancieite, from Sabato et al., 2007) form black or brown crusts, probably originated during oxygenation events, as confirmed by Fiore et al. (2000) in a similar section from Campomaggiore (Basilicata, Potenza). In the BH-e, the Mn_{EF} values are lower than in the rest of the section, even if the samples at the onset and at the end of the BH-e can show moderate Mn_{EF} values (up to ~$1.7x10^5$). The Valloneto Albian Event 1 is characterized by Mn_{EF} value of ~ $5.9x10^4$ (VAE1 in Fig. 4).

Detrital proxies

Yttrium, zirconium and aluminum are usually used to represent the terrigenous fraction of black shales, assuming that: i) Y and Zr are immobile elements located mainly in igneous rocks or clastic sediments (Bau, 1996; Pašava et al., 2017), ii) Zr and Al are contributed by and are located entirely in the siliciclastic/aluminosilicate phases (Calvert and Pedersen, 1993; Tribovillard et al., 2006). All these elements show a rough but progressive decrease upsection (Fig. 6 and Table 2). Average zirconium and aluminum concentrations are 72 ppm and 0.49 wt%, respectively. These values are substantially lower than UCC values of 190 ppm and 80400 ppm, respectively (McLennan, 2001). Yttrium concentrations range from 31 to 15 ppm, being thereby closer to the UCC value of 22 ppm (McLennan, 2001). Notably, samples within the BH-e show highly variable Zr, Al and Y contents, spanning the variability of the entire section. As a whole, there is no correlation between the detrital input and the TOC, as selected samples show variable Zr, Al and Y contents independently on their TOC content.

Fig. 5 - Dark manganese crusts on a claystone (sample V16A).

DISCUSSION

Mineralogical variability

The almost complete absence of carbonates and the widespread presence of quartz (Table 1) indicates that the depositional environment was most likely located below the Calcite Compensation Depth (CCD). This is sustained by the occurrence of radiolarites, as widely documented by the biostratigraphic micropaleontological data collected by Sabato et al. (2007). The low Y, Zr and Al concentrations in the sediments throughout the section, substantially below UCC values (Fig. 6), further indicate an overall dilution of terrigenous material with organic matter and/or siliceous radiolarian cherts, pointing to distal deep waters.

Nonetheless, we note that carbonaceous laminae locally characterize the sedimentary section deposited before (i.e., samples V16E and V20A in Table 1) and during the BH-e, although the latter were not analysed for chemistry and mineralogy. The local presence of carbonate levels is due to the occurrence of fine-grained turbiditic events (often totally or partially silicified) interrupting the normal pelagic sedimentation (Sabato et al., 2007) rather than fluctuations of the CCD.

The mineralogical variability of clay minerals (Fig. 7) shows that illite type clay is mainly present in the BH-e, whereas kaolinite and muscovite occur mostly in the lower portion of the section, before the BH-e. This variability in clay distribution can be related to changes in the depositional environment at the onset of OAE 2 and, in particular, to the triggering of a slowdown of the oceanic circulation (Scopelliti et al., 2004; 2006; Viaggi et al., 2019). This process, coupled with a distal environment under the CCD, may have caused sedimentation by decantation of fine clays (i.e. illite type), together with deposition of high amount of quartz (mainly biogenic) and may have prevented sedimentation of continental-derived material (i.e. kaolinite and muscovite).

Finally, low contents of pyrite are observed (Table 1). It is worth of note that pyrite is often absent or close to zero in the black shales related to euxinic conditions (see discussion in chapter 5.2). This aspect is likely due to the alteration of pyrite forming non-stoichiometric and poorly crystalline phases or Fe oxides (e.g. goethite).

Some inferences on redox conditions and primary productivity

Several authors showed that trace metals geochemistry of shales is a powerful tool to assess redox conditions

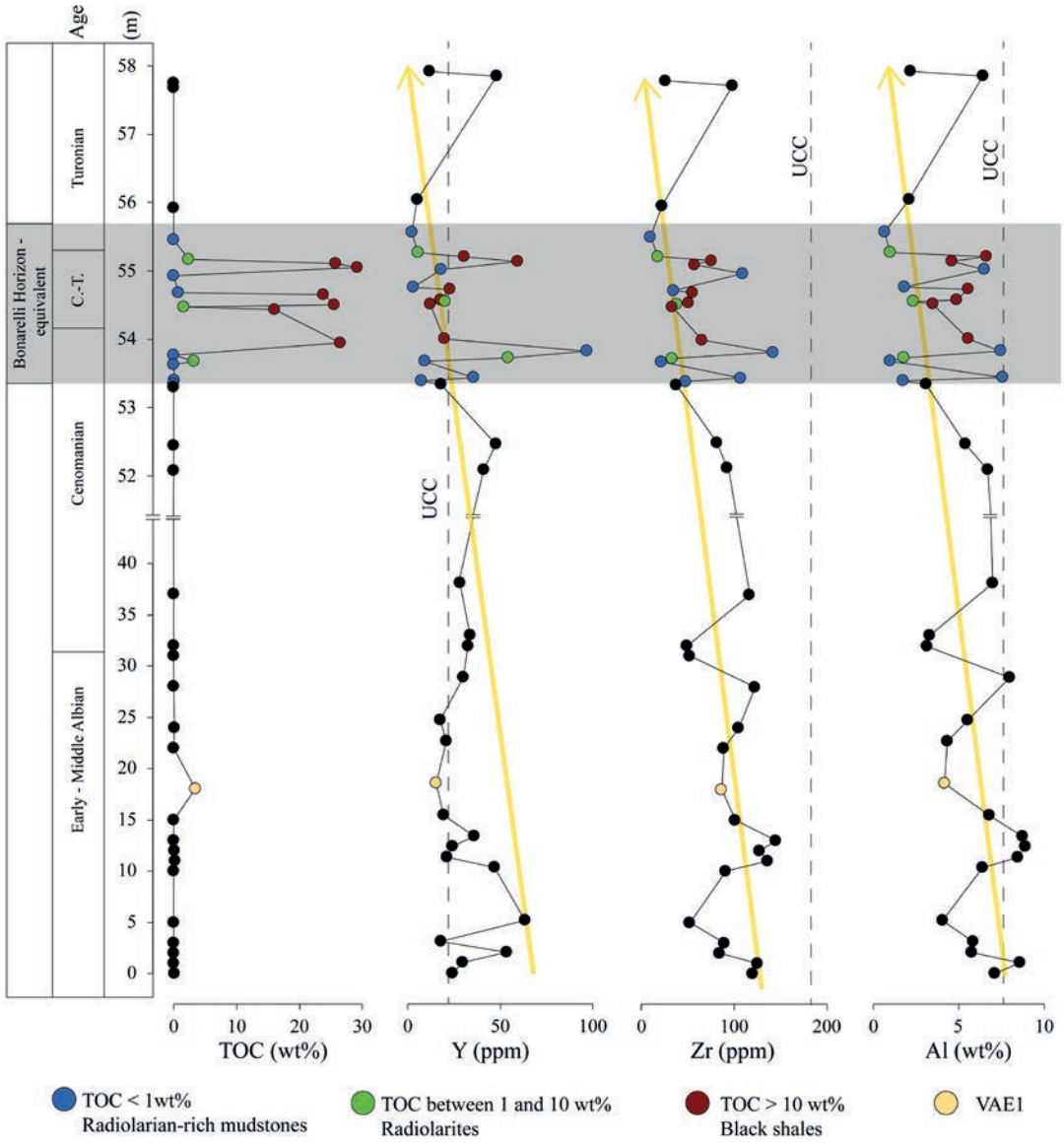

Fig. 6 - Total Organic Carbon (TOC), Y, Zr and Al values along the Fontana Valloneto Section. Vertical dashed lines represent UCC values (McLennan, 2001). VAE1 stands for "Valloneto Albian Event 1". Yellow arrows represent the decreasing trend of Y, Zr and Al.

(Tribovillard et al., 2006 and referenced therein). In particular, the gradual variability in concentrations of Redox Sensitive elements (RSEs) (i.e., V, U, Mo) in marine sediments can be used to define oxic (> 2.0 ml O_2/l H_2O), suboxic (0.2-2.0 ml O_2/l H_2O), anoxic (< 0.2 ml O_2/l H_2O) and euxinic (absence O_2 of presence of free H_2S) conditions. This is possible because under reducing conditions and in laminated and organic-rich facies, RSEs show enrichments compared to global shale or Upper Continental Crust values (hereafter UCC from McLennan, 2001). Conversely, in bioturbated, organic-poor facies deposited under oxygenated conditions, RSEs show little or no enrichments compared to the concentrations in UCC. However, Viaggi et al. (2019) by studying a late Aptian-early Campanian immature well sequence of OAEs (OAE1c, OAE1d, OAE2, OAE3) from Central Atlantic, find a covariance relationship among TOC, HI, U, S, pyrite (redox-related preservation signal), along with V, Mo, Ni, Zn, Se and P. These correlations were interpreted as nutrient-related bioproductivity signal from marine phytoplankton. The covariance pattern between nutrient-related elements complexed to kerogen and redox proxies, suggests trace metals uptake in deep-sea organic sediments during anoxic events.

An exception is represented by Mn, which is enriched under oxidizing conditions forming insoluble Mn oxides and depleted under reducing conditions.

Vanadium, molybdenum and uranium enrichment factors show positive correlations with TOC. At negligible TOC concentrations, all three elements show values close to those of the UCC (McLennan, 2001), while at high values of TOC, these elements are strongly enriched (Fig. 8).

The correlations are particularly well defined in the sediments within the BH-e, extending towards very high TOC (> 10 wt%). These TOC-rich black shales (red points in Fig. 9) are characterized by strong RSEs enrichments, confirming that reducing conditions allow both organic matter and trace metals to be preserved and fixed into the sediments (Algeo and Maynard, 2004; Tribovillard et al., 2006; Viaggi et al., 2019). In particular, Mo concentrations always higher than 25 ppm (Table 2) indicate strong euxinic conditions (Scott and Lyons, 2012).

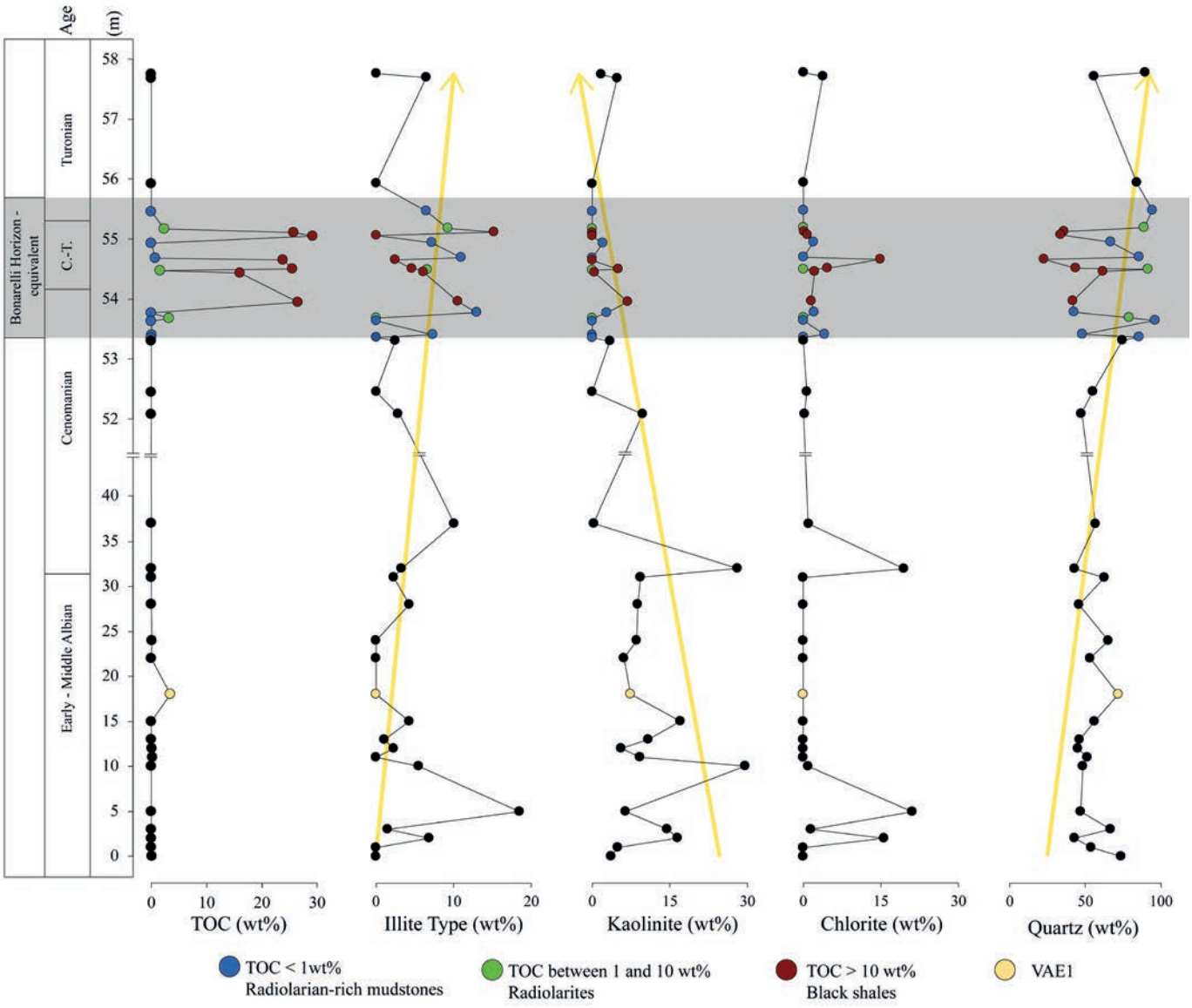

Fig. 7 - Illite type, kaolinite, chlorite, quartz contents along the section. VAE1 stands for "Valloneto Albian Event 1". Yellow arrows represent the decreasing/increasing trend for illite type, kaolinite and quartz.

The black radiolarites characterized by TOC between 1 and 10 wt% (green points in Fig. 9) show moderate Mo enrichments, with Mo values ranging between the UCC value (1.5 ppm; McLennan, 2001) and 25 ppm (Table 2), pointing toward anoxia with limited uptake of Mo (Scott and Lyons, 2012). Also, in the same levels, V and U enrichment factors show values close to or slightly higher than 1 (Fig. 9). Regarding Mn_{EF}, V29B show very high Mn, likely related to alteration of the samples (white point in Fig. 9), whereas samples V36A and $V23A_{light}$ have Mn values of ~ $14x10^3$ and ~ $34x10^3$ ppm, respectively (Fig. 9). For the latter, the MnEF are high, however, they are placed in a contest of decreasing for the sample $V23A_{light}$ and increasing for the sample V36A, indicating the development of anoxic conditions at the beginning of the BH-e and the ending of the anoxic event, respectively.

Finally, levels with TOC <1 wt% also occur within the BH-e (blue points in Fig. 9). In agreement with low contents of organic matter, these levels consist mainly of grey/yellow/red radiolarian-rich mudstones and have RSEs enrichment factors that approach 1 (blue points in Fig. 9). Also, Mn in these samples shows enrichment factors close to 1 during the BH-e deposition or higher than 1 at the onset and at the end of the anoxic event. Most likely, Mn concentrations mark the development of reducing conditions at the beginning of the BH-e and return to oxic conditions moving out of the BH-e. In addition, Gambacorta et al. (2016), describing Albian-Turonian sections containing BH-e in the Umbria-Marche Basin and the Belluno Basin (Italy), argue that during the BH-e deposition radiolarian-rich layers may form under oxic-suboxic conditions, possibly associated to a process of winnowing of the seafloor by relatively active bottom currents. Thus, it is possible that the deposition of these layers was temporarily characterized by "less reducing" (probably suboxic) periods in which the organic matter was degraded before being incorporated within the sediments.

Hence, changes in concentration of RSEs and nutrient-related elements suggest for the BH-e fluctuations in redox conditions (ranging between suboxic to euxinic) and in the primary OM productivity. Several authors relate these

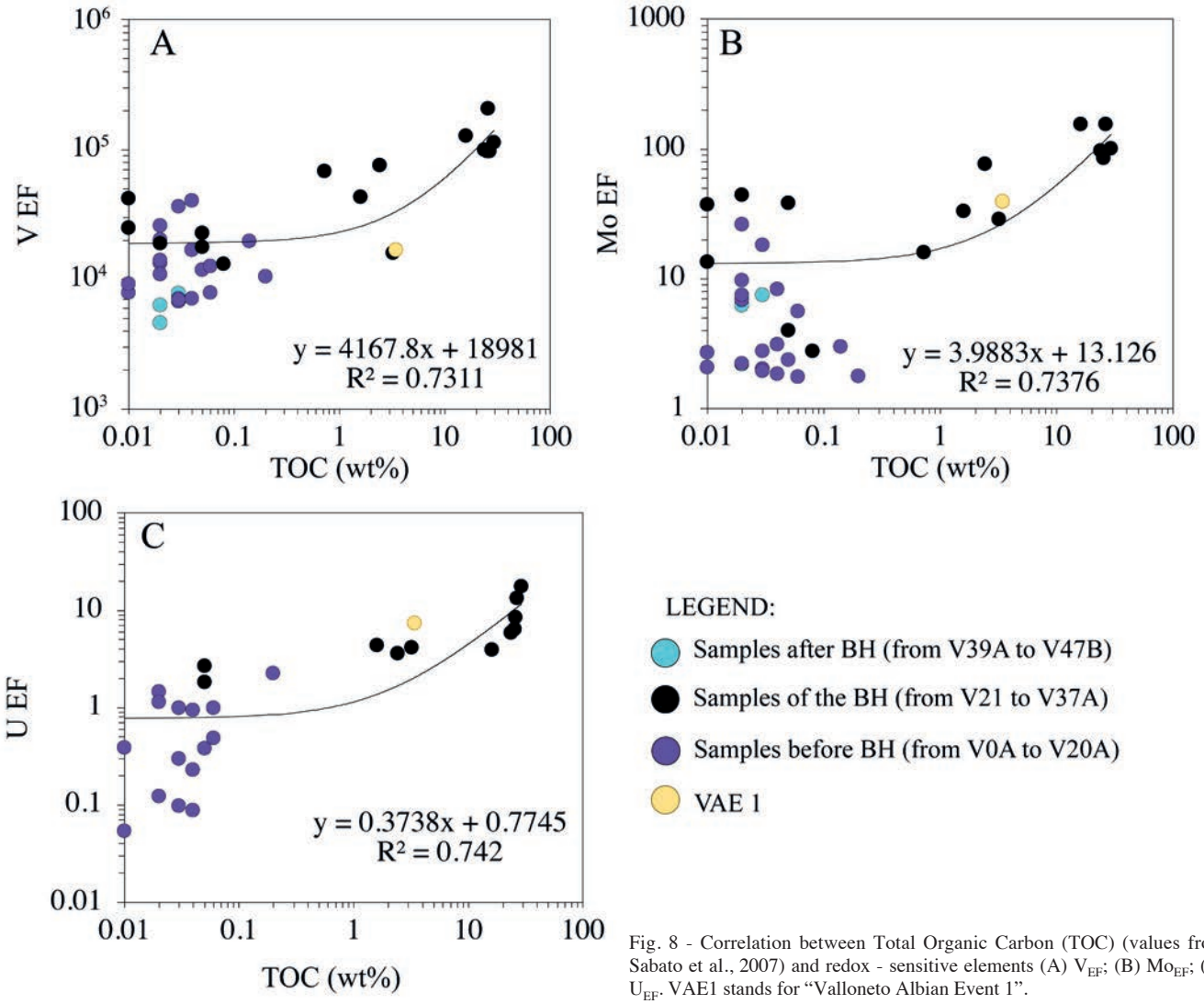

Fig. 8 - Correlation between Total Organic Carbon (TOC) (values from Sabato et al., 2007) and redox - sensitive elements (A) V_{EF}; (B) Mo_{EF}; (C) U_{EF}. VAE1 stands for "Valloneto Albian Event 1".

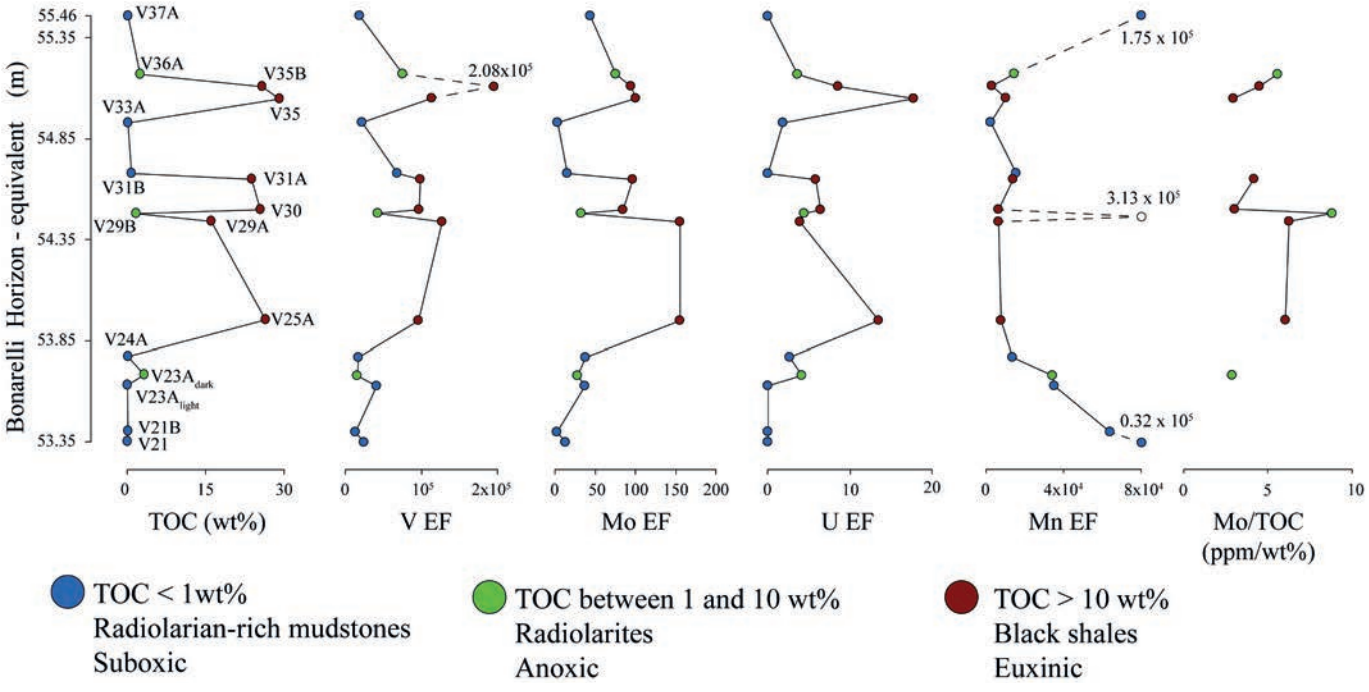

Fig. 9 - Total Organic Carbon (TOC) (data from Sabato et al., 2007), V_{EF}, Mo_{EF}, U_{EF}, Mn_{EF}, Mo/TOC (only for samples with TOC > 1wt%) values along the Bonarelli Horizon – equivalent. The white point in the Mn_{EF} graph represents an altered sample with anomalous value of Mn (V29B).

fluctuations to a strong orbital climatic forcing in which the main high productivity event was caused by a cyclicity of periods characterized by eccentricity-controlled humidity fluctuations. These events induced an increase in riverine influxes (high Rb/Al) and water stratification and, possibly, high aeolian input (high Ti/Al). Specifically, Rb is known to be present in several common minerals including mica and clay minerals and generally related to the continental weathering of granitic rocks and fluvial discharge (Rachold and Brumsack, 2001; Scopelliti et al., 2004; 2006; Kylander et al., 2011; Tanaka and Watanabe, 2015). The wind, instead, might have favored a mixing of the shallow seawater and an increase of the nutrient supply (Scopelliti et al., 2004; 2006; Galeotti et al., 2009).

In the rest of the section the RSEs enrichment factors gradually decrease towards 1, while Mn slowly increases showing high values of enrichment factor (Fig. 4), in agreement with oxigenated conditions and low TOC.

It is worth noting that the sample V13A located at 18 m from the bottom of the section (VAE1; orange point in Fig. 4) shows high TOC (~ 3.43 wt%) and enrichments in RSEs (except for V) compared to the neighboring deposits (Fig. 4), pointing toward anoxic conditions. Contrarily, Mn is enriched compared to the UCC (Mn_{EF} = ~ $59x10^3$) and HI is low (~ 220 mg HC/g TOC; Sabato et al., 2007), indicating a possible weathering of the sample that led to a decrease in HI (and probably of TOC too) and an increase of Mn compared to the original values. Due to these considerations, we can infer local anoxic conditions during the deposition of the Valloneto Albian Event 1.

Depositional environment

TOC and RSEs concentrations in the BH-e level of Fontana Valloneto section suggest that OAE2 was characterized by periods with high productivity and high preservation with redox conditions fluctuating between suboxic to strongly euxinic. Reducing conditions were recorded by other Italian sections that intersect the Bonarelli Level, although related to different mechanisms. For instance, at Bottaccione section (Umbria-Marche, Scopelliti et al., 2006), anoxic-euxinic conditions during OAE 2 were associated to high productivity and high riverine runoff, coupled with a "sluggish" oceanic circulation. Differently, at the Calabianca section (Sicily, Southern Italy) the strong OM productivity is mainly related to an efficient upwelling present along the African passive margin that, in turn, caused euxinic conditions in the entire water column (Scopelliti et al., 2004; 2006; Tribovillard et al., 2012). This difference may be related to the depositional environments that at the Bottaccione section was mid-deep pelagic (1500 – 2500 m; Arthur and Premoli Silva, 1982; Kuhnt, 1990; Scopelliti et al., 2008) and located in a complex basin along the continental margin of the Apulian block (Centamore et al., 1980; Scopelliti et al., 2006; 2008); whereas at the Calabianca section was shallow (1000 - 1500m; Catalano et al., 2002; Scopelliti et al., 2008) and located in the Southern continental margin of the Mesozoic Tethys (Scopelliti et al., 2006; 2008). In addition, during the deposition of the Bonarelli Horizon in the Bottaccione section, the low carbonates suggest a temporary rise of the CCD linked to increased water acidity as a consequence of enhanced oxidation of organic matter, whereas in the Calabianca section, carbonates contents are always high (~ 16 wt%; Scopelliti et al., 2004) indicating a shallow depositional environment (Scopelliti et al., 2006).

Based on the previous inferences, the Fontana Valloneto section could have recorded redox conditions similar to those of the Bottaccione section during the Bonarelli Horizon sedimentation, but in a different depositional environment. The lack of carbonates before, during and after the BH-e (Table 2) in fact suggests that the depositional environment was always under the CCD, and that that the entire Fontana Valloneto section was deposited in a more distal and pelagic environment compared to Bottaccione and Calabianca sections. In addition, the Fontana Valloneto BH-e contains higher TOC contents (> 10 wt%), which indicate (i) higher organic matter productivity, (ii) higher preservation and (iii) lower dilution of OM (and lower sedimentation rates) compared to the Umbrian and Sicilian basins. A combination of the three conditions seems reasonable, and sustained by high OM concentrations, enrichments of nutrient-related trace metals and RSEs (Fig. 9) and by the sedimentation of illite type clays over kaolinite and muscovite (Fig. 7), likely triggered by a slowdown of the oceanic circulation (Scopelliti et al., 2004; 2006) through a Cretaceous global long-term eustatic climax (+250 m) during OAE 2 time (Viaggi et al., 2019).

In agreement, several proxies (i.e. Ti/Al, K/Al and Rb/Al) have been analysed, in order to study in more detail the detrital input of the depositional environment during the BH-e deposition. Specifically, Rachold and Brumsack (2001) suggested that high Ti/Al values can be related to high contribution from fine-grained aeolian input, which is generally Ti-enriched. Fontana Valloneto shows Ti/Al average (Fig. 10) values of 0.06 prior to, 0.07 during and 0.05 after the BH-e that are very close to the UCC values (Ti/Al_{UCC} = 0.05; calculated after McLennan, 2001), indicating that an increase of the influx from aeolian dust occurred during the Bonarelli Horizon sedimentation.

Owing to the high affinity of K compared to Al into illite, the K/Al ratio is considered as another clastic influx proxy providing information on the detrital input derived from the fine-grained sediments (Wehausen and Brumsack, 1999; Rachold and Brumsack, 2001; Brumsack, 2006; Soua, 2013). Although K/Al ratios are generally lower than the UCC value in the Fontana Valloneto (K/Al_{UCC} = 0.35; calculated after McLennan, 2001) (Fig. 10), thereby indicating that the fine sedimentation was limited along the entire section, these ratio increase to ~ 0.30 during the BH-e, implying a temporarily increase of the fine grained supply. Finally, Rb/Al, representing the riverine input (Scopelliti et al., 2004; 2006), show an average of ~ 0.10 along the entire section (Fig. 10), that is below the UCC concentration (Rb/Al_{UCC} = 0.13; calculated after McLennan, 2001), indicating that the terrigenous flux related to the rivers was low along the entire section.

Concluding, the aforementioned detrital proxies suggest that the entire section is characterized by a fine-grained sedimentation, in agreement with the idea that the depositional environment of Fontana Valloneto was likely located in a distal deep basin with low riverine influxes from the continent.

Causes of variability in redox conditions during OAE 2

Looking in detail at the Bonarelli Horizon-equivalent, some differences can be noted between the black shales (TOC > 10 wt%) and radiolarites/radiolarian-rich mudstones (TOC < 10 wt%). Black shales (red points in Fig. 10) are generally characterized by high peaks in Ti/Al and K/Al compared to the radiolarites (green and blue points in Fig. 10) pointing toward the idea that their deposition was associated to fine grained sedimentation. It is probable that the black shales are

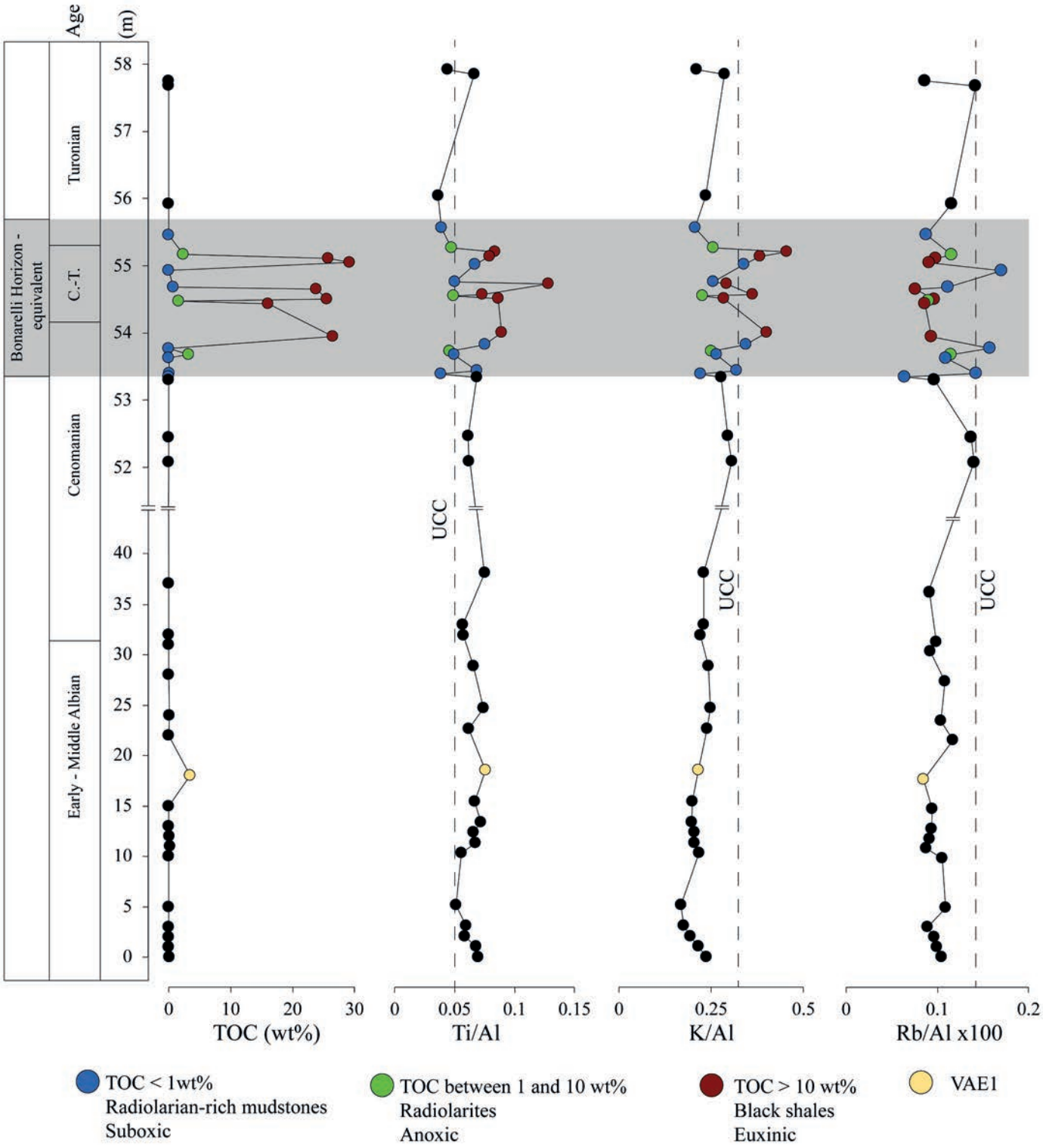

Fig. 10 - Total Organic Carbon (TOC), Ti/Al, K/Al and Rb/Al (x100) along the Fontana Valloneto Section. Vertical dashed lines represent UCC values (McLennan, 2001). VAE1 stands for "Valloneto Albian Event 1".

the results of high bioproductivity and high preservation of the OM under euxinic conditions, as testified by high TOC values and enrichments in RSEs and nutrient-related metals. This likely occurred under stagnant conditions where OM deposited together with fine grained sediments (illite and aeolian dust) through decantation. Euxinic conditions may have been promoted by degradation of high amount of OM, produced also thanks to the aeolian input that may have provided additional nutrients in surface waters. Finally, the black shales are characterized by low Rb/Al, indicating a low detrital input from rivers during their deposition. This is also in agreement with the hypothesis of Viaggi et al. (2019) where OAE 2 was associated to a global long-term eustatic climax compatible with starved conditions.

Conversely, the radiolarian-rich mudstones levels in the BH-e (green and blue points in Fig. 10) are not associated to high TOC, Ti/Al and K/Al values (Fig. 10) but to peaks in Rb/Al (Fig. 10), Zr, less Al and Y (Fig. 6), along with minor enrichments in RSEs and TOC < 10 wt%. These characteristics suggest that the decreasing OM contents are related to deposition of these layers under less reducing conditions than the black shales, during periods of enhanced riverine supply recorded by peaks in Rb/Al (Fig. 10) that may have obfuscated the aeolian signal. Accordingly, Gambacorta et al. (2016) proposed that radiolarian layers, belonging to the entire Albian-Turonian interval, can be related to oxic-suboxic periods in which the bottom currents might be relatively active. A different situation has been observed in Bottaccione section (Scopelliti et al., 2006) where the deposition of black shales during the Bonarelli Level has been related to high organic matter productivity in the photic zone in a period of intense rivers contribution that diluted the aeolian input compared to older and younger times, as suggested by high Rb/Al and low Ti/Al values (Scopelliti et al., 2004; 2006). Conversely, and similar to the Fontana Valloneto section, enhanced siliceous biogenic production (i.e. radiolarites deposition) is related to period of renewal of circulation resulting in a recycling of nutrients. Contemporaneously, an increase of oxygen to deep waters induced OM degradation as suggested by low values in Cr/Al and V/(V + Ni) ratios (Scopelliti et al., 2006).

Global implications

Based on RSEs concentrations discussed above, we showed that the OAE 2 in Fontana Valloneto section, Bottaccione and Contessa (see below) sections are characterized by suboxic-euxinic conditions (Fig. 11). A different situation is represented by other localities of the proto-Atlantic Ocean and Western Tethys during OAE 2: i.e. Calabianca section (Fig. 11; Scopelliti et al., 2004; 2006), Furlo section (Umbria - Marche, Central Italy; Fig. 11; Owens et al., 2017), Demerara Rise (Hetzel et al., 2009; Wang et al., 2016; Ostrander et al., 2017) and Cape Verde (Site 367; Westermann et al., 2014) in which strong euxinia was observed. Here, iron speciation and molybdenum isotopes suggest strongly euxinic conditions throughout the entire OAE 2. These conditions were accompanied by depletions in Mo, V and U, likely due to the global expansion of euxinia (Hetzel et al., 2009; Westermann et al., 2014; Wang et al., 2016; Ostrander et al., 2017; Owens et al., 2017). In particular, Owens et al.

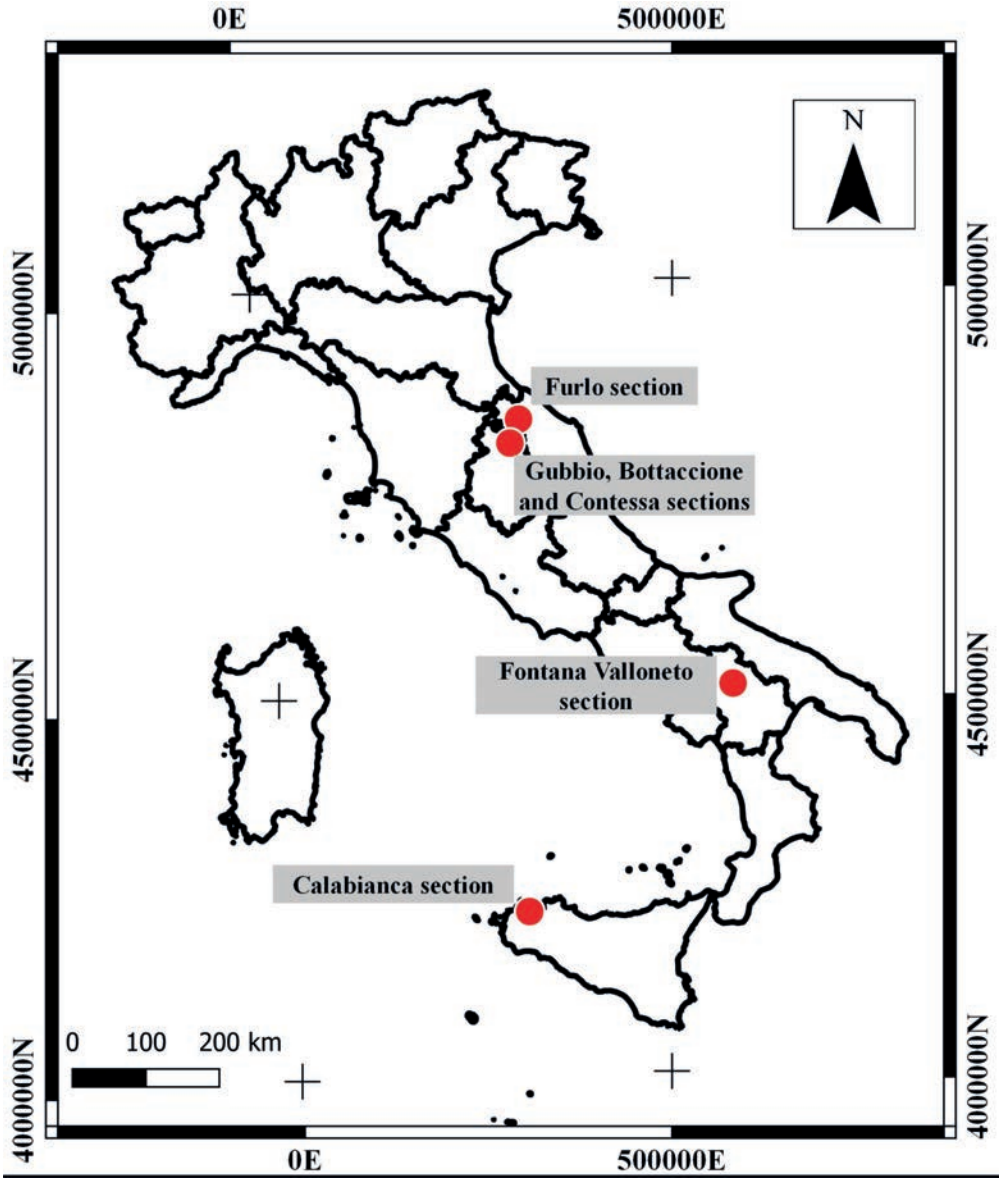

Fig. 11 - Locations of some Italian sections (Furlo, Bottaccione, Contessa, Fontana Valloneto and Calabianca sections).

(2017) suggested that section marginal marine sediments do not show strong trace-metal enrichments compared to the UCC values during OAE 2 because of overabundance of sinks (i.e., anoxic waters and sediments) in many areas of the ocean compared to the relatively small supply (of the ocean inventory). This is in agreement with Viaggi et al. (2019) observation of an OAE 2 depletion of nutrient-related elements (Mo, V), interpreted as temporary seawater "nutrient crisis" induced by starved and stagnant conditions of central Atlantic basin during the Cenomanian-Turonian eustatic climax. This trend, observed in the localities cited above (Furlo section, Demerara Rise, Cape Verde) and well documented in literature (e.g., Algeo and Maynard, 2004; Reinhard et al., 2013; Goldberg et al., 2016; Owens et al., 2016; Ostrander et al., 2017), suggests a drawdown of the global inventory of Mo in the ocean.

In addition, the Mo/TOC ratio point toward a depleted marine Mo reservoir in all these localities. Algeo and Lyons (2006) show that different Mo/TOC ratios reflect the size of Mo inventory as related to global or local factors. So, normalizing Mo to TOC allows to see relationships that do not depends on organic matter control but only on the reservoir. Mo/TOC ratios from different OAE 2 localities, compared to those of the Fontana Valloneto section (Fig. 9), are reported in Table 2. The case study presented here shows a Mo/TOC average value of 4.9 during the BH-e deposition, which is slightly higher than the other occurrences (see Table 3) and the Black Sea values (Mo/TOC average (ppm/wt%) = 4.5±1; Algeo and Lyons, 2006), which is considered the modern analogue of black shales formation during OAEs (except for Cape Verde - Site 367; see below).

Also, Algeo and Lyons (2006) showed that the Mo/TOC values in modern basins are controlled by the restriction of the basin. So, the ratio depends on the renewal time of deep waters relative to the rates of Mo uptake and the H_2S spreading into the water column. For instance, the data from Furlo section (Owens et al., 2017) reflect the sequestration of Mo by sediments under euxinic conditions that is faster than the water renewal.

Also, Pearce et al. (2008) and Algeo (2004) relate this inventory process to a massive uptake of Mo, as well of V and U, by OM-rich deposits during periods of strong euxinia. This has been observed not only during OAE 2, but also during others OAEs (e.g. Toarcian - Oceanic Anoxic Event and the Late Devonian - Early Mississippian black shale succession of the Central Appalachian Basin).

High Mo values observed in Cape Verde (Site 367) have been linked by the authors (Scott and Lyons, 2012; Tribovillard et al., 2012; Westermann et al., 2014) to the operation of Mn shuttling: variable redox conditions cause Mo to be captured and released by Mn oxides several times within the euxinic layer, accelerating its transport to the seafloor with the particulate and its fixation into the euxinic sediments. This process has been inferred also for the Bottaccione section (Scopelliti et al., 2006) and Contessa section (Westermann et al., 2014). In particular, the latter case records fluctuating conditions between anoxia and euxinia along the Bonarelli Level and in the second part of the OAE 2, δ^{98}Mo shift towards lighter values indicating a non-quantitative removal of Mo from the water column and/or the operation of a Mn shuttling. Thus, Fontana Valloneto shows very similar Mo/TOC concentrations to Cape Verde (site 367) and Bottaccione section (Table 3), pointing toward the idea that a Mn particulate shuttling may have played an important role leading to Mo enrichments. In fact, the enrichment factors of Mo and U (Mo_{EF} and U_{EF}, respectively) calculated for the Fontana Valloneto section are compatible with the particulate shuttling process, accordingly to Algeo and Tribovillard (2009), as shown in Fig. 12.

Data shown in Table 3 suggest that deep-water Mo concentrations were low in both proto-North Atlantic and Tethys Oceans, and constantly close to Fontana Valloneto section or lower than the modern euxinic restricted basin (i.e. Black Sea). Thus, the Mo and RSEs concentrations cannot be explained solely by a local depletion due to "sluggish" circulation in restricted basins. Rather, Nd isotopes from Demerara Rise (Martin et al., 2012) suggest that there was an active water exchange between the Tethys and Central and North Atlantic in the Late Cretaceous. Hence, the comparison between several OEA 2 sections around the world implies that the low Mo/TOC values - in our case associated probably also to depletion in V and U - are due to a global perturbation in redox conditions of the ocean, and the subsequent sink effect within OM-rich sediments.

CONCLUSIONS

Combination of mineralogy, TOC and geochemical data allowed to reconstruct the depositional history of Fontana Valloneto. In particular, the lack of carbonates throughout the entire sequence and a gradual decrease in Y, Zr and Al contents indicates that the Fontana Valloneto section was located in a deep distal basin (under the CCD) during the deposition of the section. In addition, our geochemical data (V, Mo, U, Mn and TOC) suggest a sudden change in redox conditions at the onset of the BH-e, which was characterized by fluctuating reducing conditions. These are suggested by three different trends:

i)- Suboxic conditions characterized by radiolarian-rich mudstones associated to TOC < 1 wt%, RSEs concentrations close to UCC values, variable Mn enrichments;

Table 3 - Overview of Mo/TOC (ppm/wt%) average values within OAE 2. Mo/TOC average values from this study are calculated only for the samples with TOC > 1wt%.

	Site	Mo/TOC (ppm/wt%)	References
Proto - North Atlantic	Demerara Rise	2	Hetzel et al. (2009)
	Cape Verde (site 367)	5	Westermann et al. (2014)
Tethys Ocean	Fontana Valloneto section	4.9	This study
	Calabianca section	2	Tribovillard et al. (2012)
	Bottaccione section	4	Tribovillard et al. (2012)
	Furlo Section	3.2	Owens et al. (2017)
	Contessa section	3	Westermann et al. (2014)

ii)- Anoxic conditions characterized by radiolarites associated to TOC between 1 and 10 wt% and little or no enrichments in RSEs and Mn;

iii)- Euxinic conditions characterized by black shales associated to TOC > 10 wt%, enrichments in RSEs and Mn values close to UCC.

Finally, comparison with other sections intercepting the OAE2 in the Tethys and in the proto-Atlantic oceans allowed to discuss two implications:

i)- The local variability within the BH-e in Fontana Valloneto indicate that black shales are associated to high TOC, Ti/Al, K/Al and enrichments in RSEs indicating high bioproductivity, stagnant conditions, fine-grained sedimentation (illite and aeolian dust) and euxinic conditions, while radiolarites/radiolarian-rich mudstones are associated to low TOC, high Rb/Al and low RSEs enrichments indicating an increase of the oceanic circulation and riverine input leading to less reducing conditions;

ii)- Mo/TOC ratio during the BH-e deposition in the Fontana Valloneto section is consistent with the values of the same ratio from other sections from the proto-Atlantic Ocean and the Mesozoic Tethys (Cape Verde and Bottaccione section, respectively), confirming the idea that global reducing conditions during OAE2 led to a depletion of the global inventory of Mo (and, likely, of V and U) due to the sink effect of euxinic waters and temporary seawater "nutrient crisis" induced by basin starved conditions associated to the Cenomanian-Turonian global long-term eustatic climax. We favour the idea that Mo depletion was a global process, instead of consequence of the marine basin restriction.

In this work, we define another Italian section intersecting the OAE 2, located in the Southern Tethys, providing a new case of study to understand the global significance of the geochemical parameters characterizing the sediments formed during these periods of strongly reducing conditions.

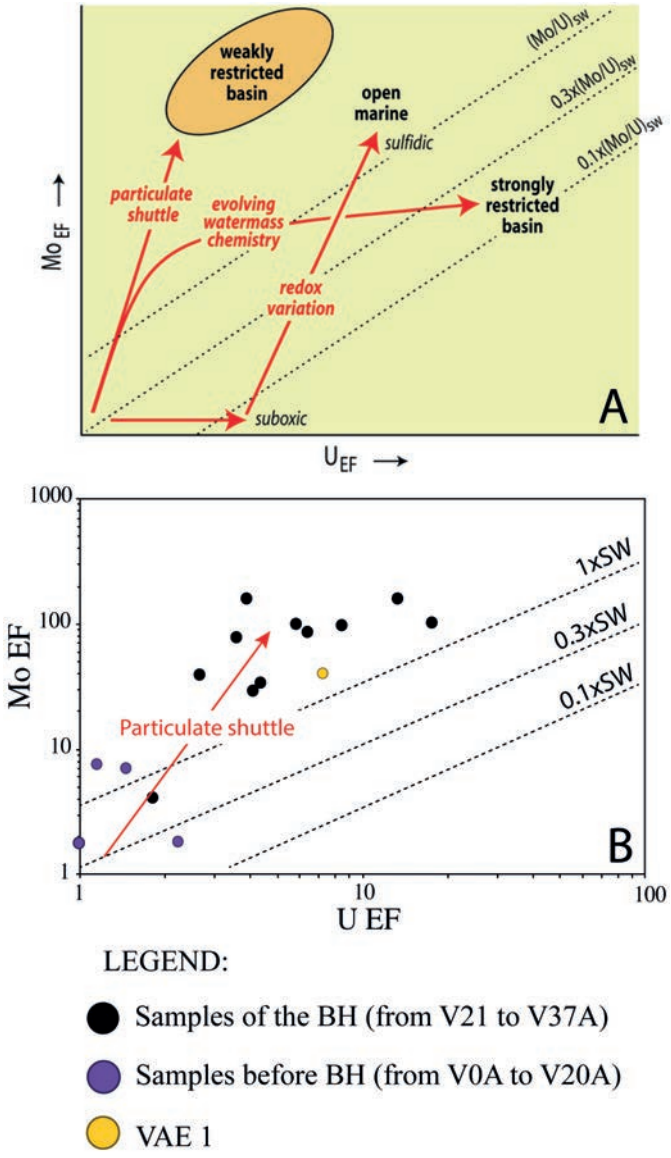

Fig. 12 - A) Model of enrichment patterns and changes in $(Mo/U)_{auth}$ ratios (from Algeo and Tribovillard, 2009). B) Cross plot of Mo and U enrichment factors for the Fontana Valloneto section (only EFs > 1 are plotted). The diagonal dotted lines represent the seawater (SW) Mo/U molar ratio of ~7.5-7.9 and fractions thereof.

ACKNOWLEDGMENTS

Two anonymous reviewers are gratefully acknowledged for their constructive comments on the manuscript. This research was supported by Eni. We thank Piernatale Casali, Flavio Riboni, Lorenzo Bianchi, Tiziano Ragazzo and Cesare Mulas who helped to acquire the data in the Eni laboratories.

REFERENCES

Algeo T.J., 2004. Can marine anoxic events draw down the trace element inventory of seawater? Geology, 32, 1057-1060. https://doi.org/10.1130/G20896.1

Algeo T.J. and Li. C., 2020. Redox classification and calibration of redox thresholds in sedimentary systems. Geochim. Cosmochim. Acta. https://doi.org/10.1016/j.gca.2020.01.055

Algeo T.J. and Lyons T.W., 2006. Mo-total organic carbon covariation in modern anoxic marine environments: implications for analysis of paleoredox and paleohydrographic conditions. Paleoceanography, 21, PA1016. https://doi.org/10.1029/2004PA001112

Algeo T.J. and Maynard J.B., 2004. Trace-element behavior and redox facies in core shales of Upper Pennsylvanian Kansas-type cyclothems. Chem. Geol., 206: 289-318. https://doi.org/10.1016/j.chemgeo.2003.12.009

Algeo T.J. and Tribovillard N., 2009. Environmental analysis of paleoceanographic systems based on molybdenum–uranium covariation. Chem. Geol., 268 (3-4): 211-225. https://doi.org/10.1016/j.chemgeo.2009.09.001

APAT, 2006. Carta Geologica d'Italia 1:50,000 - Catalogo delle Formazioni - Unità tradizionali (2). Quad. Serv. Geol. d'It., S.EL.CA., Firenze, serie III, 7(VII), pp. 382.

Arthur A., Jenkyns H.C., Brumsack H.J. and Schlanger S.O., 1990. Stratigraphy, geochemistry, and paleoceanography of organic carbon-rich Cretaceous sequences. In: R.N. Ginsburg and B. Beaudoin (Eds.), Cretaceous resources events and rhythms NATO ASI Series C., 30: 75-119. Kluwer Acad. Publ.

Arthur M.A. and Premoli-Silva I., 1982. Development of widespread organic carbon-rich strata in the Mediterranean Tethys. In: S.O. Schlanger and M.B. Cita (Eds.), Nature and origin of Cretaceous carbon-rich facies. p. 7-54. Acad. Press, New York.

Batenburg S.J., De Vleeschouwer D., Sprovieri M., Hilgen F.J., Gale A.S., Singer B.S., Koeberl C., Coccioni R., Claeys P. and Montanari A., 2016. Orbital control on the timing of oceanic anoxia in the Late Cretaceous. Clim. Past, 12: 1995-2009. https://doi.org/10.5194/cp-12-1995-2016

Bau M., 1996. Controls on the fractionation of isovalent trace elements in magmatic and aqueous systems: evidence from Y/Ho, Zr/Hf, and lanthanide tetrad effect. Contrib. Miner. Petrol., 123 (3): 323-333.

Beaudoin B., M'Ban E.P., Montanari A. and Pinault M., 1996. Lithostratigraphie haute resolution (< 20 ka) dans le Cénomanien du basin d'Ombrie-Marches. C. R. Acad. Sci., Paris, Sér. IIa, 32: 689-696.

Berner R.A., 2006. GEOCARBSULF: a combined model for Phanerozoic atmospheric O2 and CO2. Geochim. Cosmochim. Acta, 7: 5653-5664.

Blättler C.L., Jenkyns H.C., Reynard L.M. and Henderson G.M., 2011. Significant increases in global weathering during Oceanic Anoxic Events 1a and 2 indicated by calcium isotopes. Earth Planet. Sci. Lett., 309: 77-88. https://doi.org/10.1016/j.epsl.2011.06.029

Blumenberg M. and Wiese F., 2012. Imbalanced nutrients as triggers for black shale formation in a shallow shelf setting during the OAE 2 (Wunstorf, Germany). Biogeosciences, 9: 4139-4153. https://doi.org/10.5194/bg-9-4139-2012

Brumsack H.J., 2006. The trace metal content of recent organic carbon-rich sediments: implications for Cretaceous black shale formation. Palaeo. Palaeo. Palaeo., 232: 344-361. https://doi.org/10.1016/j.palaeo.2005.05.011

Butler R.W.H., Pinter P.R., Maniscalco R. and Hartley A.J., 2020. Deep-water sand fairway mapping as a tool for tectonic restoration: decoding Miocene central Mediterranean paleogeography using the Numidian turbidites of southern Italy. J. Geol. Soc., 117: 766-783. https://doi.org/10.1144/jgs2020-008

Catalano R., Lo Cicero G. and Sulli A., 2002. Geology of Sicily: an introduction. In: M. Santantonio, (Ed.), General Field Trip Guidebook, 6th Intern, Symp. on Jurassic System, September 2002, Palermo, Italy, pp. 5-20.

Calvert S.E. and Pedersen T.F., 1993. Geochemistry of recent oxic and anoxic marine sediments: implications for the geological record. Mar. Geol., 113 (1-2): 67-88.

Centamore E., Chiocchini M., Jacobacci A., Manfredini M. and Manganelli P., 1980. The evolution of the Umbrian-Marchean Basin in the Apennine section of the Alpine orogenic belt (Central Italy). In: J. Cogne and M. Slansly (Eds.), Mém. Bureau Recher. Géol. Min., 108: 289-305.

Centamore E., Chiocchini U., Jacobacci A., Lanari G. and Santagati G., 1971a. Geologia della zona nord-occidentale del F° 187 "Melfi" (Lucania). Boll. Serv. Geol. It., 91: 113-148.

Centamore E., Chiocchini U., Jacobacci A., Lanari G. and Santagati G., 1971b. Geologia della zona tra Acerenza e Avigliano (prov. di Potenza). Studi Geol. Camerti, 1: 97-118.

Ciaranfi N. and Loiacono F., 1983. Il Flysch Numidico nel quadro dell'evoluzione tettonico-sedimentaria infraoceanica dell'Appennino meridionale. Studi Geol. Geof. regioni pugliese e lucana, 16, 43 pp.

Cohen K.M., Finney S.C., Gibbard P.L. and Fan J.X., 2013. The ICS (Intern. Chronostrat. Chart). Episodes, 36: 199-204.

Dickson A.J., Jenkyns H.C., Porcelli D., Van den Boorn S. and Idiz E., 2016a. Basin-scale controls on the molybdenum-isotope composition of seawater during Oceanic Anoxic Event 2 (Late Cretaceous). Geochim. Cosmochim. Acta, 178: 291-306. https://doi.org/10.1016/j.gca.2015.12.036

Dickson A.J., Jenkyns H.C., Porcelli D., Van Den Boorn S., Idiz E. and Owens J.D., 2016b. Corrigendum to "Basinscale controls on the molybdenum-isotope composition of seawater during Oceanic Anoxic Event 2 (Late Cretaceous)". Geochim. Cosmochim. Acta, 189: 404-405, https://doi.org/10.1016/j.gca.2016.06.025

Du Vivier A.D.C., Selby D., Condon D.J., Takashima R. and Nishi H., 2015. Pacific 187Os/188Os isotope chemistry and U-Pb geochronology: synchroneity of global Os isotope change across OAE 2. Earth Planet. Sci. Lett., 428: 204-216. https://doi.org/10.1016/j.epsl.2015.07.020

Du Vivier A.D.C., Selby D., Sageman B.B., Jarvis I., Gröcke D.R., and Voigt S., 2014. Marine 187Os/188Os isotope stratigraphy reveals the interaction of volcanism and ocean circulation during Oceanic Anoxic Event 2. Earth Planet. Sci. Lett., 389: 23-33. https://doi.org/10.1016/j.epsl.2013.12.024

Eldrett J.S., Ma C., Bergman S.C., Lutz B., Gregory F.J., Dodsworth P., Phipps M., Hardas P., Minisini D., Ozkan A., Ramezani J., Bowring S.A., Kamo S.L., Ferguson K., Macaulay C. and Kelly A.E., 2015. An astronomically calibrated stratigraphy of the Cenomanian, Turonian and earliest Coniacian from the Cretaceous Western Interior Seaway, USA: implications global chronostratigraphy. Cretac. Res., 56: 316-344. https://doi.org/10.1016/j.cretres.2015.04.010

Fiore S., Piccarreta G., Santaloia F., Santarcangelo R. and Tateo F., 2000. The Flysch Rosso shales from the Southern Apennines, Italy. 1. Mineralogy and geochemistry. Per. Miner., 69 (1): 63-78.

Fornelli A., Gallicchio S. and Micheletti F., 2019. U-Pb detrital zircon ages and compositional features of Bifurto quartz-rich sandstones from Southern Apennines (Southern Italy): comparison with Numidian Flysch sandstones to infer source area. It. J. Geosci., 138 (2): 216-230. https://doi.org/10.3301/IJG.2019.02

Friedrich O., Norris R.D. and Erbacher J., 2012. Evolution of middle to Late Cretaceous oceans - A 55 m.y. record of Earth's temperature and carbon cycle. Geology, 40: 107-110. https://doi.org/10.1130/G32701.1

Galeotti S., Rusciadelli G., Sprovieri M., Lanci L., Gaudio A. and Pekar S., 2009. Sea-level control on facies architecture in the Cenomanian-Coniacian Apulian margin (Western Tethys): a record of glacio-eustatic fluctuations during the Cretaceous greenhouse? Palaeo. Palaeo. Palaeo., 276: 196-205. https://doi.org/10.1016/j.palaeo.2009.03.011

Gallicchio S. and Maiorano P., 1999. Revised stratigraphy of the Serra Palazzo formation, a Miocene foredeep turbidite succession of the Southern Apennines (Italy). Riv. It. Paleont. Stratigr., 105: 287-302.

Gallicchio S., Marcucci M., Pieri P., Premoli Silva I., Sabato L., Salvini G., 1996. Stratigraphical data from a Cretaceous claystones sequence of the "Argille varicolori" in the Southern Apennines (Basilicata, Italy). Palaeopelagos, 6: 261-272.

Gambacorta G., Bersezio R., Weissert H. and Erba E., 2016. Onset and demise of Cretaceous oceanic anoxic events: The coupling of surface and bottom oceanic processes in two pelagic basins of the western Tethys. Paleoceanography, 31 (6): 732-757. https://doi.org/10.1002/2015PA002922

Gambacorta G., Jenkyns H.C., Russo F., Tsikos H., Wilson P.A., Faucher G. and Erba, E., 2015. Carbon- and oxygen-isotope records of mid-Cretaceous Tethyan pelagic sequences from the Umbria Marche and Belluno Basins (Italy). Newsl. Stratigr., 48: 299-323.

Goldberg T., Poulton S.W., Wagner T., Kolonic S.F. and Rehkämper, M., 2016. Molybdenum drawdown during Cretaceous Oceanic Anoxic Event 2. Earth Planet. Sci. Lett., 440: 81-91, https://doi.org/10.1016/j.epsl.2016.02.006

Haq B.U., Hardenbol J.A.N. and Vail P.R., 1987. Chronology of fluctuating sea levels since the Triassic. Science, 235: 1156-1167.

Hasegawa T., 1997. Cenomanian-Turonian carbon isotope events recorded in terrestrial organic matter from northern Japan. Palaeo. Palaeo. Palaeo., 130: 251-273.

Hetzel A., Böttcher M.E., Wortmann U.G. and Brumsack H.J., 2009. Paleo-redox conditions during OAE 2 reflected in Demerara Rise sediment geochemistry (ODP Leg 207). Palaeo. Palaeo. Palaeo., 273: 302-328. https://doi.org/10.1016/j.palaeo.2008.11.005

Hetzel A., MÄrz C., Vogt C. and Brumsack H.J., 2011. Geochemical environment of Cenomanian – Turonian black shale deposition at Wunstorf (northern Germany). Cretac. Res., 32: 480-494. https://doi.org/10.1016/j.cretres.2011.03.004

I.S.P.R.A., 2017. Carta geologica in scala 1:50.000, Foglio Geologico 471 Irsina. ISPRA, Serv. Geol. d'It., Ed. System Cart. ISBN-10: 8893110636. Available online: https://www.isprambiente.gov.it/Media/carg/471_IRSINA/Foglio.html

I.S.P.R.A., in press. Carta geologica in scala 1:50.000, Foglio Geologico 470 Potenza. ISPRA, Serv. Geol. d'It. Available online: https://www.isprambiente.gov.it/Media/carg/470_POTENZA/Foglio.html

Jarvis I.A.N., Murphy A.M. and Gale A.S., 2001. Geochemistry of pelagic and hemipelagic carbonates: criteria for identifying systems tracts and sea-level change. J. Geol. Soc., 158: 685-696. https://doi.org/10.1144/jgs.158.4.685

Jenkyns H.C., 2003. Evidence for rapid climate change in the Mesozoic-Palaeogene greenhouse world. Philos. Transact. Royal Soc. London. Ser. A: Math. Phys. Engin. Sci., 361 (1810): 1885-1916. https://doi.org/10.1098/rsta.2003.1240

Jenkyns H.C., 1985. The Early Toarcian and Cenomanian-Turonian anoxic events in Europe: comparisons and contrasts. Geol. Runds., 74 (3): 505-518.

Jenkyns H.C., 2010. Geochemistry of oceanic anoxic events. Geochem. Geophys. Geosyst., 11: Q03004. https://doi.org/10.1029/2009GC002788

Jenkyns H.C., Matthews A., Tsikos H. and Erel Y., 2007. Nitrate reduction, sulfate reduction, and sedimentary iron isotope evolution during the Cenomanian-Turonian oceanic anoxic event. Paleoceanography, 22: PA3208, doi:10.1029/2006pa001355, https://doi.org/10.1029/2006PA001355

Jones C.E. and Jenkyns H.C., 2001. Seawater strontium isotopes, oceanic anoxic events, and seafloor hydrothermal activity in the Jurassic and Cretaceous. Am. J. Sci., 301: 112-149. https://doi.org/10.2475/ajs.301.2.112

Kuhnt W., Luderer F., Nederbragt S., Thurow J. and Wagner T., 2005. Orbital-scale record of the late Cenomanian-Turonian oceanic anoxic event (OAE 2) in the Tarfaya Basin (Morocco). Int. J. Earth Sci., 94: 147-159. https://doi.org/10.1007/s00531-004-0440-5

Kuhnt W., 1990. Agglutinated foraminifera of western Mediterranean Upper Cretaceous pelagic limestones (Umbrian Apennines, Italy, and Betic Cordillera, Southern Spain). Micropaleontology, 36: 297-330.

Kuroda J., Ogawa N.O., Tanimizu M., Coffin M.F., Tokuyama H., Kitazato H., and Ohkouchi, N., 2007. Contemporaneous massive subaerial volcanism and late cretaceous Oceanic Anoxic Event 2. Earth Planet. Sci. Lett., 256 (1-2): 211-223. https://doi.org/10.1016/j.epsl.2007.01.027

Kylander M.E., Ampel L., Wohlfarth B. and Veres D., 2011. High-resolution X-ray fluorescence core scanning analysis of Les Echets (France) sedimentary sequence: new insights from chemical proxies. J. Quatern. Sci., 26 (1): 109-117. https://doi.org/10.1002/jqs.1438

Lanci L., Muttoni G. and Erba E., 2010. Astronomical tuning of the Cenomanian Scaglia Bianca Formation at Furlo, Italy. Earth Planet. Sci. Lett., 292: 231-237. https://doi.org/10.1016/j.epsl.2010.01.041

Lu Z., Jenkyns H.C. and Rickaby R.E.M., 2010. Iodine to calcium ratios in marine carbonate as a paleo-redox proxy during oceanic anoxic events. Geology, 38: 1107-1110. https://doi.org/10.1130/G31145.1

Martin E.E., MacLeod K.G., Jiménez Berrocoso A. and Bourbon E., 2012. Water mass circulation on Demerara Rise during the Late Cretaceous based on Nd isotopes. Earth Planet. Sci. Lett., 327-328; 111-120. https://doi.org/10.1016/j.epsl.2012.01.037

McLennan S.M., 2001. Relationships between the trace element composition of sedimentary rocks and upper continental crust. Geochem., Geophys., Geosyst., 2 (4): https://doi.org/10.1029/2000GC000109

Mostardini F. and Merlini S., 1986. L'Appennino centro-meridionale. Sezioni geologiche e proposta di modello strutturale. Mem. Soc. Geol. It., 35: 177-202.

Ogniben L., 1969. Schema introduttivo alla geologia del confine calabro-lucano. Mem. Soc. Geol. It. 8: 453-763.

Ostrander C.M., Owens J.D. and Nielsen S.G., 2017. Constraining the rate of oceanic deoxygenation leading up to a Cretaceous Oceanic Anoxic Event (OAE 2: ~ 94 Ma). Sci. Adv., 3 (8). https://doi.org/10.1126/sciadv.1701020

Owens J.D., Lyons T.W., Li X., Macleod K.G., Gordon G., Kuypers M.M., Anbar A., Kuhnt W. and Severmann, S., 2012. Iron isotope and trace metal records of iron cycling in the proto North Atlantic during the Cenomanian-Turonian oceanic anoxic event (OAE-2). Paleoceanography, 27 (3). https://doi.org/10.1029/2012PA002328

Owens J.D., Lyons T.W., Hardisty D.S., Lowery C.M., Lu Z., Lee B. and Jenkyns H.C., 2017. Patterns of local and global redox variability during the Cenomanian - Turonian Boundary Event (Oceanic Anoxic Event 2) recorded in carbonates and shales from central Italy. Sedimentology, 64: 168-185. https://doi.org/10.1111/sed.12352

Owens J.D., Reinhard C.T., Rohrssen M., Love G.D. and Lyons T.W., 2016. Empirical links between trace metal cycling and marine microbial ecology during a large perturbation to Earth's carbon cycle. Earth Planet. Sci. Lett., 449: 407-417. https://doi.org/10.1016/j.epsl.2016.05.046

Pašava J., Frýda J. and Štorch P., 2017. Trace element variations as a proxy for reconstruction of palaeoenvironmental changes during the Late Aeronian faunal and carbon isotope perturbations: new data from the peri-Gondwanan region. Geol. Quart., 61 (1): 91-98. https://doi.org/10.7306/gq.1313

Patacca E., Scandone, P., Bellatalla M., Perilli N. and Santini U., 1992. The Numidian-sand event in the Southern Apennines. Mem. Sci. Geol. Padova, 43: 297-337.

Pearce C.R., Cohen A.S., Coe A.L. and Burton K.W., 2008. Molybdenum isotope evidence for global ocean anoxia coupled with perturbations to the carbon cycle during the Early Jurassic. Geology, 36 (3): 231-234, https://doi.org/10.1130/G24446A.1

Pearce M.A., Jarvis I. and Tocher B.A., 2009. The Cenomanian-Turonian boundary event, OAE2 and palaeoenvironmental change in epicontinental seas: new insights from the dinocyst and geochemical records. Palaeo. Palaeo. Palaeo., 280: 207-234, https://doi.org/10.1016/j.palaeo.2009.06.012

Pescatore T., Di Nocera S and Matano F. with the contributions of Ciampo G, Di Donato V., Esposito P. and Riviello A. (in press). Note illustrative della Carta Geologica d'Italia alla scala 1:50.000, F° 470 Potenza. ISPRA, Serv. Geol. d'It., 140 pp. Available online: https://www.isprambiente.gov.it/Media/carg/note_illustrative/470_Potenza.pdf

Pescatore T., Renda P., and Tramutoli M., 1988. Rapporti tra le unità lagonegresi e le unità sicilidi nella media valle del Basento, Lucania (Appennino Meridionale). Mem. Soc. Geol. It., 41: 353-361.

Pescatore T.S. and Senatore M., 1986. A comparison between a present-day (Taranto Gulf) and a Miocene (Irpinian Basin) foredeep. IAS Spec Pub 8: 169-182.

Pescatore T.S., Renda P., Schiattarella M. and Tramutoli M., 1999. Stratigraphic and structural relationships between Meso-Cenozoic Lagonegro basin and coeval carbonate platforms in southern Apennines, Italy. Tectonophysics, 315: 269-286.

Pieri P., Gallicchio S., Sabato L., and Tropeano M. with the contribution of Boenzi F., Lazzari M., Marino M. and Vitale G., 201. Note illustrative della Carta Geologica d'Italia alla scala 1:50.000, F° 471 Irsina. ISPRA, Serv. Geol. d'It., Ed. System Cart, 112 pp. ISBN-10: 8893110636. Available online: https://www.isprambiente.gov.it/Media/carg/note_illustrative/471_Irsina.pdf.

Pogge Von Strandmann P.A.E., Jenkyns H.C. and Woodfine R.G., 2013. Lithium isotope evidence for enhanced weathering during Oceanic Anoxic Event 2. Nat. Geosci., 6: 668:672. https://doi.org/10.1038/ngeo1875

Rachold V. and Brumsack H.J., 2001. Inorganic geochemistry of Albian sediments from the Lower Saxony Basin NW Germany: palaeoenvironmental constraints and orbital cycles. Palaeo. Palaeo. Palaeo., 174 (1-3): 121-143. https://doi.org/10.1016/S0031-0182(01)00290-5

Reinhard C.T., Planavsky N.J., Robbins L.J., Partin C.A., Gill B.C., Lalonde S.V., Bekker A., Konhauser K.O. and Lyons T.W., 2013. Proterozoic ocean redox and biogeochemical stasis. Proc. Natl. Acad. Sci., 110: 5357-5362. https://doi.org/10.1073/pnas.1208622110.

Sabato L., Gallicchio S., Pieri P., Salvini G. and Scotti P., 2007. Cretaceous anoxic events in the argilliti e radiolariti di Campomaggiore unit (Lagonegro-Molise basin, southern Italy). Boll. Soc. Geol. It., Spec. Issue. 7: 57-74.

Sageman B.B., Meyers S.R. and Arthur M.A., 2006. Orbital time scale and new C-isotope record for Cenomanian- Turonian boundary stratotype. Geology, 34: 125-128. https://doi.org/10.1130/G22074.1

Schlanger S.O. and Jenkyns H.C., 1976. Cretaceous oceanic anoxic events: causes and consequences. Geol. Mijnb., 55: 179-184.

Schlanger S.O., Arthur M.A., Jenkyns H.C. and Scholle P.A., 1987. The Cenomanian-Turonian Oceanic Anoxic Event, I. Stratigraphy and distribution of organic carbon-rich beds and the marine δ13C excursion. In: J. Brooks and A.J. Fleet (Eds.), Marine petroleum source rocks. Geol. Soc. London Spec. Publ., 26: 371-399.

Scholle P.A. and Arthur M.A., 1980. Carbon isotope fluctuations in Cretaceous pelagic limestones; potential stratigraphic and petroleum exploration tool. A.A.P.G. Bull., 64: 67-87.

Scopelliti G., Bellanca A., Coccioni R., Luciani V., Neri R., Baudin F., Chiari M. and Marcucci M., 2004. High-resolution geochemical and biotic records of the Tethyan "Bonarelli Level" (OAE 2, Latest Cenomanian) from the Calabianca-Guidaloca composite section, nortwestern Sicily, Italy. Palaeo. Palaeo. Palaeo., 208: 293-317. https://doi.org/10.1016/j.palaeo.2004.03.012

Scopelliti G., Bellanca A., Erba E., Jenkyns H.C., Neri R., Tamagnini P., Luciani V. and Masetti D., 2008. Cenomanian-Turonian carbonate and organic-carbon isotope records, biostratigraphy and provenance of a key section in NE Sicily, Italy: Palaeoceanographic and palaeogeographic implications. Palaeo. Palaeo. Palaeo., 265 (1-2): 59-77. https://doi.org/10.1016/j.palaeo.2008.04.022

Scopelliti G., Bellanca A., Neri R., Baudin F. and Coccioni R., 2006. Comparative high-resolution chemostratigraphy of the Bonarelli Level from the reference Bottaccione section (Umbria-Marche Apennines) and from an equivalent section in NW Sicily: Consistent and contrasting responses to the OAE2. Chem. Geol., 228 (4): 266-285. https://doi.org/10.1016/j.chemgeo.2005.10.010

Scott C. and Lyons T.W., 2012. Contrasting molybdenum cycling and isotopic properties in euxinic versus non-euxinic sediments and sedimentary rocks: Refining the paleoproxies. Chem. Geol., 324: 19-27. https://doi.org/10.1016/j.chemgeo.2012.05.012

Soua M., 2013. Siliceous and organic-rich sedimentation during the Cenomanian-Turonian Oceanic Anoxic Event (OAE 2) on the northern margin of Africa: an evidence from the Bargou area, Tunisia. Arab. J. Geosci., 6 (5): 1537-1557. https://doi.org/10.1007/s12517-011-0434-0

Takashima R., Nishi H., Huber B.T. and Leckie M., 2006. Greenhouse world and the Mesozoic Ocean. Oceanography, 19: 82-92.

Tanaka K. and Watanabe N., 2015. Size distribution of alkali elements in riverbed sediment and its relevance to fractionation of alkali elements during chemical weathering. Chem. Geol., 411: 12-18. https://doi.org/10.1016/j.chemgeo.2015.05.025

Tribovillard N., Algeo T.J., Baudin F., and Riboulleau A., 2012. Analysis of marine environmental conditions based onmolybdenum-uranium covariation: Applications to Mesozoic paleoceanography. Chem. Geol., 324: 46-58. https://doi.org/10.1016/j.chemgeo.2011.09.009

Tribovillard N., Algeo T.J., Lyons T.W. and Riboulleau A., 2006. Trace metals as paleoredox and paleoproductivity proxies: an update. Chem. Ggeol., 232 (1-2): 12-32. https://doi.org/10.1016/j.chemgeo.2006.02.012

Turgeon S. and Brumsack H.J., 2006. Anoxic vs dysoxic events reflected in sediment geochemistry during the Cenomanian-Turonian Boundary Event (Cretaceous) in the Umbria-Marche Basin of central Italy. Chem. Geol., 234: 321-339: https://doi.org/10.1016/j.chemgeo.2006.05.008

Viaggi P., Scotti P., Previde Massara E., Knezaurek G., Menichetti E., Piva A., Torricelli S. and Gambacorta G., 2019. Paleoceanographic evolution of mid-Cretaceous paleobioproductivity and paleoredox chemometric signals. Conference abstr. and presentation. 3rd Intern. Congr. Stratigraphy, STRATI 2019, July 2019, Milan. https://doi.org/10.13140/RG.2.2.32655.94886

Voigt S., Erbacher J., Mutterlose J., Weiss W., Westerhold T., Wiese F., Wilmsen M. and Wonik T., 2008. The Cenomanian-Turonian of the Wunstorf section (North Germany): global stratigraphic reference section and new orbital time scale for Oceanic Anoxic Event 2. Newsl. Stratigr., 43: 65-89: https://doi.org/10.1127/0078-0421/2008/0043-0065

Wang X., Reinhard C.T., Planavsky N.J., Owens J.D., Lyons T.W. and Johnson T.M., 2016. Sedimentary chromium isotopic compositions across the Cretaceous OAE2 at Demerara Rise Site 1258. Chem. Geol., 429: 85-92. https://doi.org/10.1016/j.chemgeo.2016.03.006

Westermann S., Vance, D., Cameron V., Archer C. and Robinson S.A., 2014. Heterogeneous oxygenation states in the Atlantic and Tethys oceans during Oceanic Anoxic Event 2. Earth Planet. Sci. Lett., 404: 178-189. https://doi.org/10.1016/j.epsl.2014.07.018

Received, September 10, 2020
Accepted, November 13, 2020
First published online, December 9, 2020